

Hierarchically structured functional materials: Synthesis strategies for multimodal porous networks*

Xiao-Yu Yang^{1,†}, Yu Li^{1,2}, Arnaud Lemaire¹, Jia-Guo Yu², and Bao-Lian Su^{1,2,‡}

¹Laboratory of Inorganic Materials Chemistry (CMI), University of Namur (FUNDP), 61, rue de Bruxelles, B-5000 Namur, Belgium; ²State Key Laboratory of Advanced Technology for Materials Synthesis and Processing, Wuhan University of Technology, Luoshi Road 122, Wuhan 430070, China

Abstract: Hierarchically porous materials displaying multimodal pore sizes are desirable for their improved flow performance coupled with high surface areas. In the last five years, a tremendous amount of research has focused upon the synthesis and applications of hierarchically porous materials. This review aims to open up a new avenue of research in this exciting field. At first, recent progress in the synthesis of hierarchically porous materials, targeted through templating methods, is reviewed. These synthesis methods involve a supermolecular assembly of amphiphilic polymers or surfactants combined with second surfactant systems or with macrotemplates such as solid particles, liquid drops, and air bubbles. The preparation procedures using surfactants combined with other chemical or physical methods, controlled phase-separation, or template replication will also be discussed. Subsequently, an innovative procedure concerning the self-formation of hierarchically porous materials is thoroughly examined. This self-formation procedure is based on a self-generated porogen mechanism. Porogens such as alcohol molecules can be precisely controlled at the molecular level to design new hierarchically porous materials. Most of these synthesis methods allow an easy and independent adjustment to the multiporosity of a material, i.e., its micro-, meso-, and macroporosity.

Keywords: hierarchically porous materials; micro-, meso-, macropore porogens; self-formation phenomenon of porous hierarchy; templating synthesis.

INTRODUCTION

In the chemical industries, the pretreatment of educts, their chemical conversion into valuable products, and the purification of the resulting product mixtures in downstream processes are traditionally carried out by sequential independent operations. In fact, one desired product from precise reagents is often prepared by a multireaction with the production of a series of intermediates. Each step needs a defined catalyst with one precise porosity and one specific functionality. The desired intermediate is often mixed with other by-products and will be separated from this mixture by a complex series of processes including cooling, compression, absorption, adsorption, drying, and distillation. By obtaining this inter-

*Paper based on a presentation at the International Symposium on Novel Materials and their Synthesis (NMS-IV) and the 18th International Symposium on Fine Chemistry and Functional Polymers (FCFP-XVIII), 15–18 October 2008, Zhenjiang, China. Other presentations are published in this issue, pp. 2253–2424.

[†]Chargé de recherche, Fonds National de Recherche Scientifique (FNRS), 5 Rue d'Egmont, B-1000, Bruxelles, Belgium

[‡]Corresponding author: Tel.: +32-81-724531; Fax: +32-81-725414; E-mail: bao-lian.su@fundp.ac.be

mediate at high purity, the optimal conversion and selectivity of the next step can be guaranteed, thus making separation critical. Hence, several catalysts and separation processes have to be used to reach the final desired product through such multistep reactions. As industry strives for improvements in efficiency and cost reductions (based on the economy of raw materials and the overconsumption of energy), the demand for a reduction in reaction and separation steps must be acted upon. In many cases, the performance of the classical chemical process can be significantly improved by integratively coupling different process units. Ideally, the multistep reaction can be realized in one reactor without any separation process using a single nanocatalyst which possesses hierarchical porosities and multifunctionalities, thus enabling a series of reactions to be achieved successively in a cascade, i.e., the product of one reaction can be the reagent of the next reaction without the need for separation and purification since the catalyst used possesses a sieving capacity owing to the presence of multiple porosities.

The great challenge that remains is to fabricate hierarchically micro-, meso-, macroporous materials with controlled individual pore size, porous structures, and functionalities.

Recent developments in templating chemistry based on supramolecular chemistry, colloidal chemistry, surfactant chemistry, and sol-gel chemistry, has expanded the synthetical methodology available whether chemical or biological such that metal-ligand binding, hydrogen bonding, and π - π interactions can now be exploited to enable the synthesis of ever-larger molecules and nanostructured materials with a remarkable degree of control. A great deal of progress has recently been made in the fields of ordered porous materials with uniform channel dimensions that can be adjusted over a wide range of length scales owing to templating chemistry. Different modes of templating were studied in depth and classified in terms of synthesis strategies of hierarchical materials. The distinction between a template and a reagent is that a template intervenes in the macroscopic geometry of the reaction rather than in the intrinsic chemistry. The template provides instructions for the formation of a single porous material from a reactant or reactants which would otherwise have the potential to assemble and react in a variety of ways. Changing the template should result in a different reactant assembly and consequently a different porous material. In general, after the template has directed the formation of the material, it is removed to yield a template-free porous material, although this does not occur when the template is an integral part of the structure it helps to form. Templating agents can be rigid and control porosity through the partitioning of space, or in the case of structure-directing agents, by relying on differences in miscibility and the creation of chemical gradients as a means of inducing pores. It is now well known that small amine molecules can control micropore (<2 nm) formation in zeolites, while surfactant assemblies [1,2] and more recently block copolymers (BCs) [2] can control the formation of mesoporous (2–50 nm) inorganic materials. Finally, macroporous (>50 nm) inorganic materials have been formed through the lost wax casting of templates [2]. These materials with unimodal pore sizes have been widely used in various fields such as catalysis, separation, drying processes, drug delivery, optics, optoelectronics, etc. However, the improvement of chemical processes and the design of integrative green chemical syntheses need more sophisticated and hierarchically porous materials.

It is envisaged that by incorporating macropores into meso-/microporous materials, the properties of both the meso-/microporous network and the macropores could be exploited simultaneously. Hierarchical materials containing both interconnected macro-/mesoporous structures or additional micropores have enhanced properties compared to materials with unimodal pore sizes due to increased mass transport through the material as well as maintaining a specific surface area of a similar value to that of fine pore systems [4–18]. Consequently, they have been the subject of recent investigations. A multitude of wet chemistry routes to hierarchically porous materials have recently been developed. For instance, dual and multiple surfactant templates have enabled the formation of hierarchically porous structures that have porosities on the 1- and 1000-nm length scales. The synthesis strategy extends to the use of a secondary template, in addition to the original surfactant, such as secondary micelles, small solid particles, liquid drops, and gas bubbles, supramolecular aggregates, and biomaterials. The possibility of combining the single surfactant-assisted procedure with supplementary chemical and/or

physical methods has also been explored in the quest for hierarchically porous materials, for example, the control of procedural (synthesis and aging) conditions, phase separation and post-treatment, or the introduction of structural units with their own inherent porosity. There are some special templated synthesis strategies that produce novel hierarchically porous materials, for example, the control of phase separation in the synthesis of zeolites with hierarchically porous structures and template replication in the synthesis of carbons with hierarchically porous structures. An innovative self-formation procedure has been thoroughly studied and used to synthesize hierarchically porous materials. This self-formation procedure is based on a self-generated porogen mechanism. Porogens such as alcohol molecules can be precisely controlled at the molecular level to design new hierarchically porous materials.

In this review, we refine and expand the templated-synthesis classifications to embrace many new approaches that are now available. We illustrate these approaches with examples from the literature and with self-formation syntheses, finally we attempt to elucidate the phenomena that lead to efficient templating. This review is divided into two parts. The first focus is on the external templating strategies that lead to the formation of hierarchically porous materials. We will first describe the use of dual and multiple templates in hierarchically porous material synthesis. A section will be concentrated on single micelle templates combined with supplementary chemical or physical methods. The last section of this part will treat the synthesis of hierarchical porous materials with two important chemical compositions. The second part deals with recent reports about a new and innovative self-formation phenomenon that can be exploited to target porous hierarchies. The formation mechanism and its application to the preparation of highly sophisticated hierarchically porous and highly advanced functional materials are discussed.

THE USE OF DUAL AND MULTIPLE TEMPLATES IN HIERARCHICALLY POROUS MATERIAL SYNTHESIS

Dual micellar templating approach

In this topic, most of the examples of bimodal mesoporous systems were based on adding a BC and a relatively small sized surfactant or cosolvent to the sol-gel solution. Coppens and co-workers reported the fabrication of bimodal mesoporous silica in two steps: first, a primary mesoporous (≈ 2 nm) material was prepared hydrothermally using a surfactant (cetyl trimethylammonium bromide, CTABr) with a comparatively small molecular structure as a template, then the second pore system (16–50 nm, dependent on solvent) was introduced via a hydrothermal treatment of the synthesized MCM41 materials in the presence of a BC surfactant (P123) [19]. A hysteresis loop around $P/P_0 = 0.8$ – 0.98 was also observed besides a flat hysteresis loop at 0.4 – 0.55 in the isotherms. The larger mesopores are very big (about 20 nm), and their distribution is quite broad. However, in all these cases, structural control was difficult, and most of these bimodal mesoporous materials lack a well-defined pore structure on at least one length scale in terms of pore shape or size. The proposal that the second, larger porosity was generated by the surfactant templating is quite questionable due to the very broad pore size distributions. Interparticular voids could be the origin of the secondary porosity. The discussion remains open. Significant progress in this field was made by Antonietti and Goltner [20] using the “nanocasting” methodology, that is, liquid-crystal templating under acidic conditions. Antonietti subsequently reported the combination of a special small fluorosurfactant with “KLE” $[\text{H}(\text{CH}_2\text{CH}_2\text{CH}_2(\text{CH})\text{CH}_2\text{CH}_3)_x-(\text{OCH}_2\text{CH}_2)_y\text{OH}]$ and “SE” [poly(styrene)-poly(ethylene oxide)] copolymers, which introduced small mesopores between the larger spherical mesopores in a certain range of concentrations, but only in a limited concentration range [21].

Hydrocarbon BC templates can mix with a fluorinated hydrocarbon for simultaneous nanocasting to generate bimodal porous materials. In fact, the fluoro-/hydrocarbon mixture is known to form separated micelles [22–24], as long as both surfactants have sufficient size, since fluorocarbons usually do not mix with hydrocarbons. The mixture of these micelles allowed the concurrent templating of silica by

two independent, self-organized templates. The special feature of this fluoro-/hydrocarbon template mixture to form two individual micellar species under all conditions was evidenced by mutual structural cross-influence (Fig. 1). By careful analysis of pore architectures by gas sorption measurements and transmission electron microscopy (TEM) of the final porous silica, parts of the phase diagrams could be established, independent of the relative template concentration. For the KLE and OTN [$\text{CF}_3(\text{CF}_2)_{6-16}\text{C}_2\text{H}_4\text{-EO}_{4-5}$] mixture, miscibility over the whole range of compositions was identified. For high KLE content, a mixed micellar phase where the two different micelles were packed in some type of organized array was identified. For all other compositions, the mutual presence of surfactants lowers the order, and mixed micellar phases with liquid structures are observed. At ratios approaching 1:1, the liquid mixture can undergo “crystallization”, and the coexistence of two highly organized liquid-crystal phases is clearly identified by TEM experiments. Similar results were obtained by Grosso and Linden, where the synthesis is based on the use of a mixture of two surfactants as structure-directing agents, the non-ionic triblock-co-polymer F127 [$(\text{EO})_{106}(\text{PO})_{70}(\text{EO})_{106}$] and the cationic fluorocarbon surfactant IC-11 [$\text{C}_8\text{F}_{17}\text{CH}_2\text{OHCH}_2\text{NH}(\text{C}_2\text{H}_5)_2\text{Cl}$] [25].

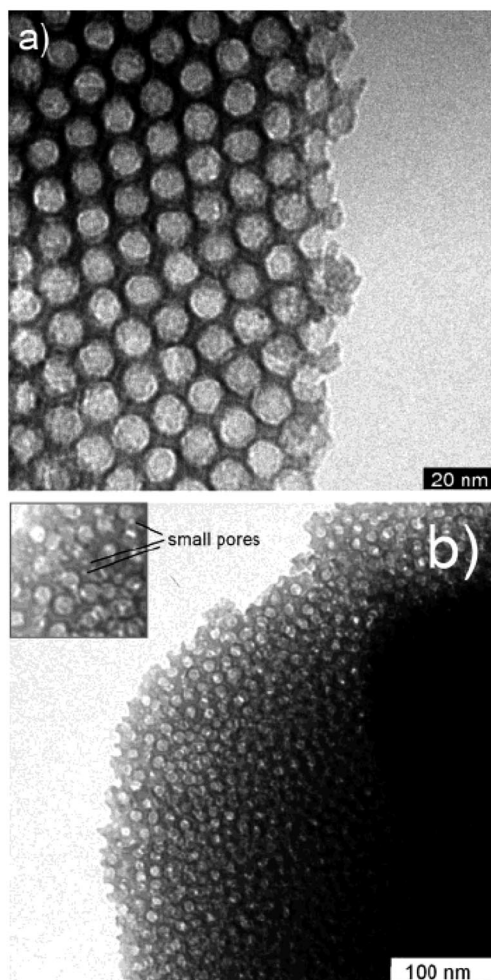


Fig. 1 TEM pictures of samples KLE-1 (a) and KLE-2 (b). As the OTN [$\text{CF}_3(\text{CF}_2)_{6-16}\text{C}_2\text{H}_4\text{-EO}_{4-5}$] content increases, the ordering of the sample decreases (b). For the sample KLE-2, the small pores generated by the OTN oligomer can be visualized between the KLE pores (see the inset) [21].

Next, another family of cotemplates, ionic liquids (ILs), was developed due to their unique templating behavior, based on the distinct polarizability of the headgroups, leading to highly ordered pore systems [26–30]. In particular, ILs showed a significantly stronger tendency toward self-aggregation and tolerance toward perturbations in supramolecular templating. This particular property of ILs was therefore expected to help to avoid phase separation of the template and the polymer within the sol-gel process. In this way, a bimodal super-microporous and macroporous silica material was obtained using poly(styrene) (PS) bead packing and an amphiphilic IL simultaneously employed as templates [31]. The wall architecture of the ordered cubic structure of the macropores (around 175 nm) is made up of a perfectly ordered supermicroporous (around 1.3 nm) lamellar phase. Trimodal meso-/macroporous silica was prepared using PS beads to create macropores, a BC (KLE) for large mesopores and an IL (1-hexadecyl-3-methylimidazolium chloride) for small mesopores [32]. The macropore size is 360 nm with a wall thickness of 100 nm, and the wall texture of the macroporous silica contains two distinguishable types of pores, both different sizes (large spherical mesopores of ca. 12 nm and small elongated mesopores of 2–3 nm). No phase separation of BC and IL was observed, with the small mesopores being located in the walls of the larger pores. It is claimed that the synthesis failed with other ionic surfactants such as CTABr. The Brunauer–Emmett–Teller (BET) surface area of such trimodal porous silica is $244 \text{ m}^2 \text{ g}^{-1}$, and the total porosity amounts to ca. $0.33 \text{ cm}^3 \text{ g}^{-1}$.

A systematic study of hierarchical materials synthesized using aqueous surfactant mixtures has recently been realized [33]. This study of the combination of various BCs (F127, KLE) and SE with smaller surfactants (P123, $\text{C}_{16}\text{mimCl}$, and CTAB) revealed that hierarchical bimodal mesoporous architectures could only be obtained by using BCs with a strong hydrophilic/hydrophobic contrast, such as KLE and SE, giving rise to pores between 6 and 22 nm. Furthermore, the IL $\text{C}_{16}\text{mimCl}$ appeared to have advantageous templating properties, resulting in 2–3 nm pores being located between the BC mesopores, whereas phase separation was observed for Pluronics and CTAB used as small templates. Thereby, the study also provided general insight into the mixing and co-self-assembly behavior of BCs and ionic surfactants in water and confirmed the special templating properties of ILs, as recently proposed. In addition to the bimodal mesoporosity, additional tunable macroporosity was created by the presence of PS or poly(methyl methacrylate) spheres, leading to well-defined trimodal hierarchical pore architectures with the small pores being located in the walls of the larger pores (Fig. 2). As a major improvement, due to the pore hierarchy, these large-pore materials showed relatively large surface areas and pore volumes, and the size of the densely packed macropores could even be decreased down to 90 nm.

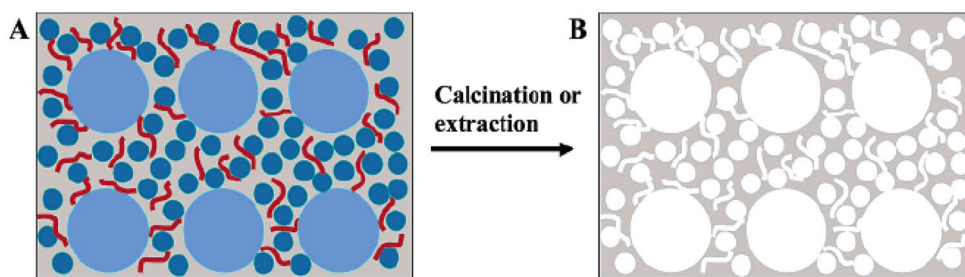


Fig. 2 General templating approach to obtain trimodal hierarchical porous materials, (A) Hybrid material (gray, silica; blue, polymer colloid; dark blue, BC micelle; red, IL micelle). (B) Corresponding silica material after calcination or extraction of templates [33].

Small solid particles as additional templates to micelle templating

Colloidal crystals as additional templates

Synthesis of the trimodal porous material described above is a significant synthesis strategy used in the preparation of hierarchical oxides, the PS colloid beads are usually considered as small solid particles with at least one characteristic dimension in the range of a few tens of nanometers to one micrometer. The combination of surfactant and colloidal crystal templating methods offers an efficient way for the construction of ordered and interconnected micro–macro-, meso–macroporous architectures [14,34–36]. Colloidal latex spheres, all having the same diameter, can be self-aggregated in a regular fashion, then the mixture of the inorganic precursors and surfactant (or copolymer) micellar solution is allowed to infiltrate the interstitial spaces between the spheres. This is followed by condensation and crystallization of the inorganic precursors. The removal of the surfactant and latex spheres, by either high-temperature calcination or solvent extraction, leads to the formation of 3D ordered micro–macro- or meso–macroporous materials (Fig. 3). The macroporous walls are composed of micro- or mesopores, and both pore types can be interconnected. Such hierarchical materials of various compositions, including titania [34], silica [20,34,37,38], niobia [34], and silica–alumina [39], have been reported. The multiple-scale structural organization formed makes it possible to tune the physical properties of the materials over a wide range of chemical compositions. Furthermore, by using two colloidal crystals of a size identical to the desired pore diameters, bimodal 3D macroporous silica structures can be synthesized. Luo et al. [37] synthesized cubic 3D ordered macroporous (140 nm) and binary macroporous (140, 80 nm) silica structures with ordered mesoporous (7.7 nm) walls by using cubic close-packing PS spheres as templates, of either one or two different sizes, respectively, and the triblock copolymer P123 as a mesostructure-directing agent.

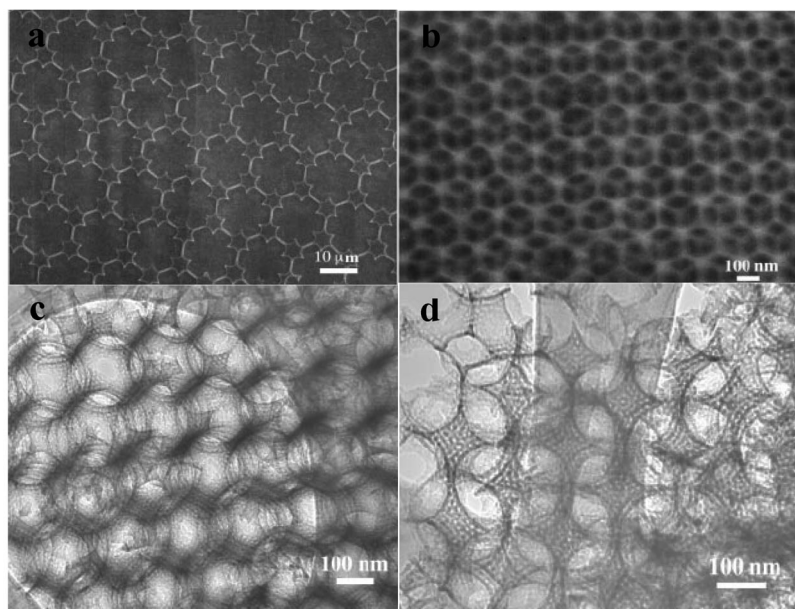


Fig. 3 SEM images (a and b) and TEM images (c and d) of hierarchically ordered mesoporous silica, displaying that organization over three discrete characteristic dimensions, and the framework of the macroporous skeleton is made up of ordered cubic mesoporous silica with an ordering length [34].

A silicate having a bimodal meso–macropore size distribution can be made by the sedimentation–aggregation technique [40], in which the gel for the synthesis of a mesophase was generated by

self-assembly of the surfactant and the silica precursor. This mixture infiltrated the voids of the agglomerated PS particles. Random packing of latex beads covered with silica occurred after the addition of latex spheres to a mixed solution of cetyltrimethylammonium chloride/hydroxide and tetraethylorthosilicate, resulting in an eggshell-type macrostructure morphology with an MCM-48-type cubic mesophase [41]. It has also been demonstrated that mixing latex beads with micellar surfactant solution before adding the inorganic source could produce a relatively uniform dispersion of macropores in the mesoporous MCM-48 materials [41]. Using this method, skeletal-structured biporous silicates with both an MCM-41 mesophase and a skeletal macrophase having an ordered array can be prepared (Fig. 4) [42]. The macrostructured MCM-41 (MS-MCM-41), synthesized after impregnation of latex spheres as a controlling step and calcination of the polymer and surfactant, showed a superior 3D ordered macroporous structure extending from several to hundreds of micrometers. The mesoporous phase located between the walls of the macropores contained the same structure as MCM-41, having a BET surface area above $1200 \text{ m}^2 \text{ g}^{-1}$, with a pore volume of about $1.27 \text{ cm}^3 \text{ g}^{-1}$. The specific volume of MS-MCM-41, accounting for both meso- and macropores, was estimated to be $7.9 \text{ cm}^3 \text{ g}^{-1}$, using a simple density measurement. Figure 4 proposes a plausible mechanism for the formation of skeletal macrostructures. The PS beads are coated with silicate primary particles, and then the doughnut-type building blocks are formed in the interstices of adjacent PS spheres through the drying and shrinking of the silica precursor solution. These building units are expanded and arranged into the face-centered cubic (fcc) close-packed PS bead particles, and the skeletal structure of MS-MCM-41 is obtained after calcination of PS spheres. The inner space of the doughnut-type building block might make the interconnecting channels between macropores.

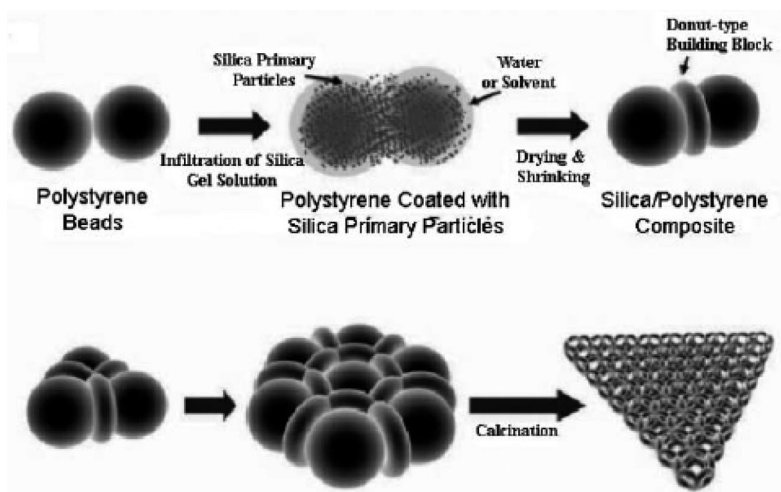


Fig. 4 Plausible schematic mechanism for the formation of skeletal-macrostructured MCM-41 [42].

The advantage of this method, despite template sacrifice, is that organic functional molecules, such as a dye, can be directly incorporated into the framework of meso-/macroporous materials. For example, mesostructured silica functionalized with the dye moiety (2,4-dinitrophenylamine) has been prepared with the control of the hierarchical pore architecture [36]. Co-condensation of tetraethoxysilane and 3-(2,4-dinitrophenylamino)propyltriethoxysilane was used to covalently couple the organic chromophore to the wall structure of a silica mesophase formed by surfactant templating of CTAB. This process was spatially patterned on the macroscale by confining the evaporation-induced precipitation of reactants within the regular voids of a colloidal crystal, comprising 140-nm-sized PS spheres. The removal of the latex and surfactant templates by extraction produced a hierarchically ordered organo-

functionalized silica meso-/macrophase. Fourier transform-infrared (FT-IR) and UV-vis diffuse reflectance spectra indicated the intact and covalent link of chromophore groups into the mesostructured silica network of the hierarchical structure. This method is also extended to many other organosilane moieties tailored to specific applications such as selective chromatographic supports for combinatorial chemistry, ferrocene-based devices in electrochemical sensors, dye-based pH sensors, and rhodium/ruthenium-based organometallic complexes for catalysis [43]. Highly dispersed polyoxometalate clusters could also be incorporated in the hybrid structures of 3D ordered macroporous silicas with mesoporous walls during direct synthesis, and these functionalized materials were demonstrated to exhibit catalytic activity for the epoxidation of cyclooctene with an anhydrous $\text{H}_2\text{O}_2/t\text{-BuOH}$ solution at room temperature [44]. Sen et al. [44,45] synthesized a series of hierarchically ordered porous silica composites with ordering on three different scales of pore size by using latex spheres and triblock copolymers (Pluronic F127 and P123) as templates in the presence of cosurfactants (n-alcohols) in an acidic medium. The silica materials obtained consisted of 3D ordered macropores (200–800 nm) with interconnecting, uniform-sized (70–130 nm) windows, where the walls of these macropores consisted of mesostructured pores (3–8 nm), as well as a significant microporosity (<2 nm), presenting a macro-, meso-, microporous structure with a 3D interconnectivity. The formation of windows is due to the close-packed arrangement of PS spheres (touching points). The meso- and microporosities are generated by micelle formation of the EO-PO-EO BC in the presence of a cosurfactant such as butanol or pentanol. The surface area and mesopore volume of the materials were low ($46 \text{ m}^2 \text{ g}^{-1}$, $0.053 \text{ cm}^3 \text{ g}^{-1}$) when the PS latex was removed by direct calcination at $550 \text{ }^\circ\text{C}$, while a high total surface area of $531 \text{ m}^2 \text{ g}^{-1}$ was obtained after removal of the latex by toluene extraction followed by calcination at $450 \text{ }^\circ\text{C}$.

On the basis of high-resolution 3D TEM, a thorough understanding of the monoliths of the meso-/macroporous materials templated by colloidal crystals was described in detail as a function of the synthesis parameters [46]. This study revealed the special alignment of the surfactant induced by the 3D confinement of colloidal crystals, especially for cylindrical micelles, which could be aligned either in parallel or perpendicular to the sphere surfaces.

Meanwhile, some other small solid particles, such as inorganic salts, ice crystals, polymer aggregates, and biomaterials, can be added during synthesis to enable the creation of macroporous structures.

Inorganic salts and ice crystals as additional templates

3D meso-macrostructured sponge-like silica membranes have been synthesized by a multiphase process of acid-catalyzed silica sol-gel chemistry in the presence of inorganic salts and self-assembling BCs [47]. Inorganic salts play an important role in the formation of the meso-macro silica structures that are grown at the interface of inorganic salt solution droplets. The meso-macrostructured silica network can be varied, depending on the electrolyte strength of the inorganic salts and the amphiphilic BC structure-directing agents. The macropore dimensions are established by the sizes of the salt solution droplets, such as NaCl, LiCl, KCl, NH_4Cl , or NiSO_4 , which can be adjusted by regulating the evaporation rate of the solvent. At the interstices separating the electrolyte droplets, amphiphilic BC species assemble in the presence of silica to form well-ordered composite mesophases. The morphology of the silica membrane can be modified by changing the concentration of the inorganic salt, although inorganic salt crystals were inevitably co-grown with the silica membrane.

A very innovative and inventive method was developed by Nishihara et al. to prepare ordered macroporous silica, a silica gel microhoneycomb (SMH), using micrometer-sized ice crystals as a template [48]. This is based on the phenomenon that when hydrosols, hydrogels, or aqueous slurries of metal oxides or polymers are quickly frozen by immersing them into a cold bath, micrometer-sized ice spheres grow inside their matrices as a result of thermally induced phase separations. These ice spheres then play the role of a template in the formation of 3D interconnected macroporous metal oxides or polymers. When precursor hydrogels, which are freshly gelled and which contain an adequate quantity of solid components, are unidirectionally frozen under conditions where the pseudo-steady-state growth

of ice crystals can continue, an array of polygonal ice rods with fairly uniform diameters grows in parallel to the freezing direction. After the removal of the ice template by elevating the temperature, large monolithic materials with ordered macropores are obtained (Fig. 5). The straight macropores have a polygonal cross-section and are parallel to the freezing direction. Besides their ordered macroporosity, micro- and mesopores develop inside the honeycomb walls through the freeze-drying of SMHs soaked in *tert*-butyl alcohol. It was found that the macropore size of the SMHs can be controlled by changing the rate of immersion into a cold bath and also the freezing temperature, without changing the micro- and mesoporosity of their honeycomb walls. The thickness of the honeycomb walls was affected by the SiO₂ concentration and the macropore size. The porosity of the honeycomb walls could be controlled to be microporous as well as mesoporous, by a hydrothermal treatment of the as-prepared SMHs in basic aqueous solutions. Moreover, SMHs with developed mesopores showed a higher stability against heat treatment. The method developed by Nishihara et al. is thus quite versatile for the preparation of hierarchically porous materials with a variety of chemical compositions.

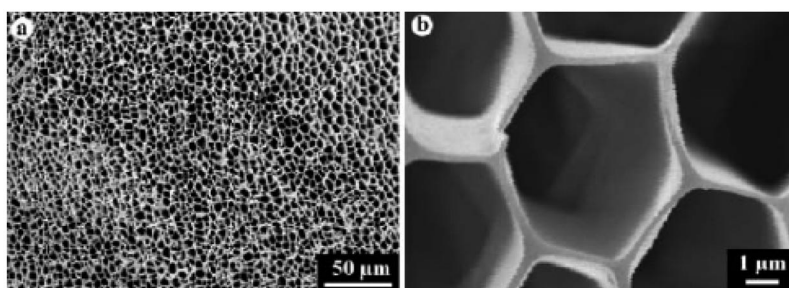


Fig. 5 SEM images of the cross-sections of SMHs prepared by ice-templating [48].

Macroporous polymers as additional templates

Cellulose acetate and polyamide membranes have been used as templates in the formation of macroporous oxide networks [49]. Infiltration of the silica/amphiphile solution within the porous structure of these membranes and its subsequent gelation results in a cast of the original membrane. Removal of both the membrane template and the porogen (amphiphilic supramolecular aggregates) by calcination leaves the amorphous silica film with a bimodal, interconnected meso-/macroporous structure (Fig. 6) [50]. The surface area and total pore volume of the inorganic films vary from 473 to 856 m² g⁻¹, and 0.50 to 0.73 cm³ g⁻¹, respectively, depending on the choice of template and porogen. The channel-like macropore assembly gives good mass transport and accessibility to the pore systems, whereas the mesopore system provides a large surface area, which is required for catalysis and separation. Other membranes made of cellulose derivatives, including cellulose nitrate, mixed cellulose esters, and regenerated cellulose, can also be employed as templates for the fabrication of bicontinuous macroporous inorganic oxide films with controlled geometry. Furthermore, applying an external electric field to a polyacrylamide hydrogel could lead to the creation of a template matrix with aligned interstitial voids of approximately 10 nm in diameter. The mesoporous silica monoliths with oriented macroporous channels were then produced by the immersion of this electric-field-oriented hydrogel monolith in neat tetramethylorthosilicate, and subsequent hydrolysis, condensation, and calcination to remove the organic phase [51]. The mesoporosity was supported by a nitrogen-adsorption isotherm of type IV with a distinct hysteresis loop of type H3, characteristic slit-type pores with average pore diameter 8.6 nm resulted from the aggregation of plate-like particles. The material had a low density of 0.806 g cm⁻³ and a BET surface area of 337 m² g⁻¹ with a pore volume of 0.73 cm³ g⁻¹.

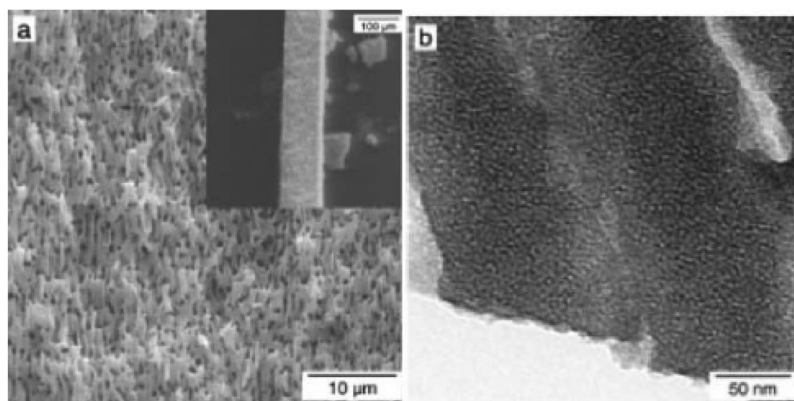


Fig. 6 (a) SEM and (b) TEM images of the meso-/macroporous silicas obtained using cellulose acetate membrane and polyoxyethylene (10) lauryl ether (C12E10) porogen [50].

Biomaterials as additional templates

For the preparation of porous inorganic materials with hierarchical structures, a rich variety of biological structures with complex morphologies have been used as sophisticated templates. Typical examples of natural biological templates include bacterial threads [52], echinoid skeletal plates [53], eggshell membranes [54], insect wings [55], pollen grains [56], plant leaves [57,58], wood celluloses [59,60], protein aggregates [61], and spider silk [62]. Since these natural biological templates offer beautiful and abundant hierarchical architectures, and are inexpensive and environmentally benign, they have attracted much interest in the construction of novel hierarchical inorganic materials.

The bacterial superstructure, consisting of a thread of coaligned multicellular filaments of *Bacillus subtilis* [52], was used to extend the length scale of inorganic material patterning by template-directed mineralization (Fig. 7) of the interfilament spaces. Ordered macroporous fibers of either amorphous silica or ordered mesoporous silica MCM-41 were produced. The inorganic macrostructures consist of a macroporous framework of 500-nm-wide channels with curved walls of either silica or mesoporous silica, 50–200 nm in thickness, showing a structural hierarchy on both the meso- and macroscopic length scales.

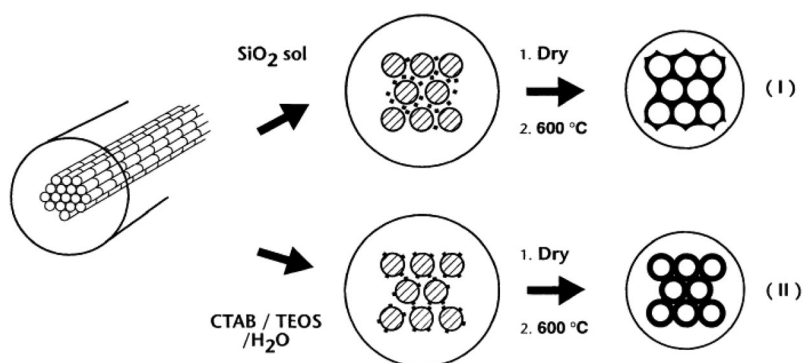


Fig. 7 Scheme showing two routes to the formation of organized macroporous inorganic frameworks using bacterial superstructural templates [52].

Natural wood has highly anisotropic cellular structures, which can be used as a hierarchical template to generate porous ceramics by deposition of a ceramic phase within the wood interstices or the infiltration of the ceramic into the unoccupied void space [59,60]. Mineralization of wood cellular structures using a surfactant-templated sol-gel solution at different pH values allows for the formation of either positive or negative replicas with a porous hierarchy. At low pH, silicic acid is coated onto the inner surface of the wood's cellular structure, and it penetrates the pores from which degraded lignin and hemicellulose have leached, to form a positive replica, while at high pH the precipitating silica particles clog the cells and pit structures due to fast condensation, forming a negative replica of wood [59]. The cell walls consist of surfactant-templated, ordered hexagonal mesopores. Moreover, wood was also used as both a carbon precursor and a hierarchical template for SiC synthesis. Mineralized wood with silica in acidic conditions followed by carbothermal reduction in argon resulted in the formation of a hierarchical SiC adopting a wood cellular structure [63]. All wood cellular structures were generally maintained, and wood cell walls were composed of crystalline SiC nanoparticles (200–700 nm). The specific surface area of the final cellular SiC ceramics was 60–100 m² g⁻¹, where the pore sizes were randomly distributed from nanometers to micrometers. Wood cellular structures of SiC materials were stable up to 1400 °C in air.

The cuttlebone is a highly organized internal shell structure constructed from aragonite (CaCO₃) in association with a chitin organic matrix. The shell has a chamber-like architecture in the form of mineralized sheets arranged in parallel layers and separated by S-shaped pillars, and has been shown to be template-ordered chamber-like macroporous chitin–SiO₂ composites [64]. Using chitosan as a template, meso-/macroporous siliceous fibrous material could be synthesized via a hydrothermal hydrolysis of sodium silicate [65], although the siliceous walls of the macropores (570 nm in radius) were micro-/mesoporous with a broad and polymodal distribution. This structure may be due to the aggregation of the hydrated chitosan helices in bundles of parallel fibers with different sizes and also the gelation of the system.

Starch gel templating was also performed to produce hierarchically sponge-like micro-, meso-/macroporous monoliths of silicalite and meso-/macroporous TiO₂ [66], where the macroporosity was generated by self-assembled nanoparticle building blocks. Non-ordered macropores in the size range 0.5–50 μm were achieved by varying the amount of starch and the starch: silicate ratio.

The use of dextran as a sacrificial template makes it possible to fabricate metallic and metal oxide sponges [67]. By heating pastes of the polysaccharide dextran containing metal salts to temperatures between 500 and 900 °C, self-supporting macroporous frameworks of silver, gold, and copper oxide, as well as composites of silver/copper oxide or silver/titania were prepared. Magnetic sponges were similarly prepared by replacing the metal salt precursor with preformed iron oxide (magnetite) nanoparticles. Solid colloidal particles as additional templates to micelle templating have been largely used to generate larger pores in hierarchically porous materials. Both macro- and meso(micro)pore sizes can be easily and independently adjusted. The most significant drawback of this synthesis strategy is the removal of solid colloidal templates by calcination or solvent extractions, which can perturb the well-organized macrostructure formed.

Small liquid drops and air bubbles as additional templates combined with micelle templating

Small liquid drops as additional templates

The method of emulsion templating [68–70] is perhaps the most general and has been used to produce macroporous titania, silica, and zirconia with pore sizes from 50 nm to several micrometers, although most of those reported materials are a disordered macroporous solid without meso- or microporosity. As the liquid drops of emulsion, such as oil, are deformable, macroscopic samples are able to accommodate stresses that arise during gelation and shrinkage [70]. Samples made using rigid spheres, by contrast, tend to break into small pieces that are seldom larger than a few hundred micrometers. In ad-

dition, emulsification conditions can be adjusted to produce droplets with different mean sizes which are typically in the micrometer range. This can be done to a large extent independently of the self-assembling BC species used to direct the structure of the mesopores. This advantage means that emulsion templating is often used in combination with micelle templating to construct hierarchically porous materials. This allows a direct and independent control of macro- and mesopore dimensions, so the final pore structures can be tailored to different diffusion and reaction conditions. The introduction of mesoporosity into a macroporous structure by a surfactant emulsion-mediated synthesis has been reported [71,72]. The room-temperature synthesis of a macro-/mesoporous silica material fabricated during the natural creaming process of an oil-in-water emulsion containing surfactant (CTAB) has been described [72]. The material obtained has 3D interconnected macropores with a strut-like structure (Fig. 8) similar to meso-cellular silica foams with mesoporous walls of worm-hole structure, i.e., macrocellular foams, which have a high surface area of about $800 \text{ m}^2 \text{ g}^{-1}$ with narrow mesopore size distribution. However, their formation mechanism is not properly understood. It is also demonstrated that mesoporous silica could be obtained using either a low oil (mesitylene) concentration with slow stirring or synthesis at alkaline pH, while faster stirring at low oil concentration produced mesocellular silica foam [71]. Disordered macro-/mesoporous silica composites with various wall thickness and interconnectivity were obtained using intermediate to high oil concentrations. Cooper and co-workers reported the synthesis of hierarchically porous emulsion-templated polymer/silica composite beads by the sedimentation polymerization of a high internal phase emulsion (HIPE) [73]. High surface area silica beads with an average bead diameter of 1.34 mm and a high pore volume ($5.68 \text{ cm}^3 \text{ g}^{-1}$) were prepared. The interconnected macroporous structure was obtained by calcinations of the composite structures. Carn et al. reported a simple method to prepare hierarchically textured macroporous silica monoliths, with organized vermicular-type mesoporosity by the use of a double template, i.e., direct emulsion at the macroscale and micellar templates at the mesoscale [74]. The monolithic materials obtained had typical polymerized HIPE (poly-HIPE)-type interconnected macroporous textures with polydisperse cell and window sizes within the micrometer range. Their texture can be tuned by varying either the pH of the continuous aqueous phase, the emulsification process, or the oil (dodecane) volume fraction. pH conditions have been shown to be an important factor in controlling the final monolith textures, also the oil-water interface seems to promote the inorganic condensation process.

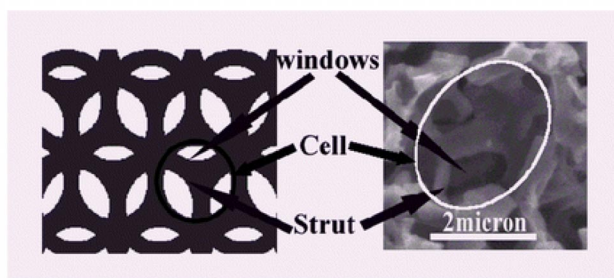


Fig. 8 Scheme and SEM image of strut-like structure in the meso-/macroporous silica synthesized by natural creaming process of an oil-in-water emulsion [71].

Mesostructured titania possessing an unusual macroporous interior, was spontaneously synthesized in an ethanolic solution of surfactant $\text{C}_{16}(\text{EO})_{10}$ containing a small quantity of water (Fig. 9) [75]. The resulting particles had quite a thick shell, and the core had a sponge-like macroporous structure with a uniform pore size gradient, such that the macropore sizes increase progressively from the shell layer to the core. Both the shell layers and the macroporous framework of the core have a disordered wormhole-like mesoporous structure comprised of a TiO_2 nanoparticle assembly. It is proposed that this

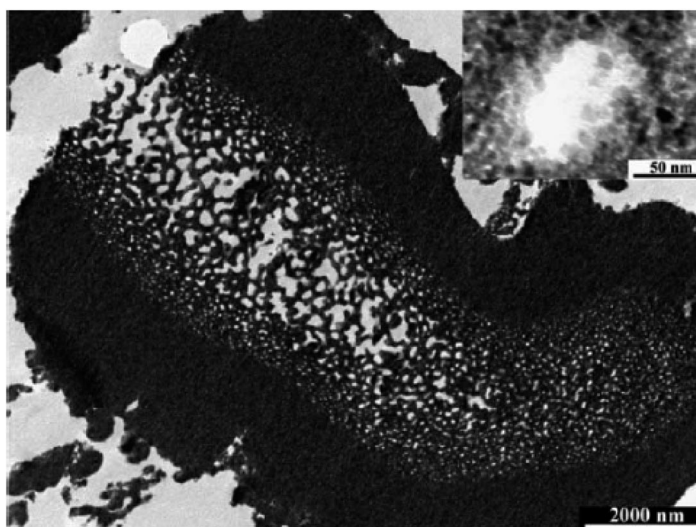


Fig. 9 Cross-section TEM images of hierarchically mesostructured titania with an interior macroporous structure [75].

hierarchical structure might be formed by combining a reverse micelle (“quasi-reverse emulsion” [76]) templating pathway with a conventional surfactant templating technique of a hybrid composite mesostructured phase. However, further study demonstrated that the surfactant molecules only play a role in the control of mesoporosity and not in the formation of this kind of hollow core/dense mesostructured shell. The formation mechanism is discussed further in the section about the self-formation procedure.

The addition of NaCl to a niobium ethoxide/amine aqueous system can result in gel vesicle templating, yielding a macro-/mesoporous niobium oxide [77]. It was emphasized that the salt was essential for surfactant vesicle formation to occur before the creation of a macro-/mesoporous niobium oxide with macropore sizes in the 200–300 nm range. This process was regarded as a ligand-assisted vesicle templating strategy. The macropore sizes of these niobium oxides were not altered by the different sized preformed vesicles, suggesting a cooperative macropore assembly mechanism rather than one involving preformed vesicles. The proposed mechanism is also questionable. The role of the surfactant and the possible formation of large vesicles, leading to the formation of meso-/macroporous materials, will be clarified in the following sections.

Small air bubbles as additional templates

Macroskeletal mesoporous silicate foams with open-cell randomly shaped macrovoids on the (sub)millimeter scale have been prepared from metastable PEO-surfactant air-liquid foams induced by strong stirring under neutral aqueous conditions [78]. It was claimed that the macroscale morphologies were tuned by changing the turbulence of the reaction media, which is certainly a very difficult parameter to control. Since then, a bubbling process has been proposed to produce air-liquid foams [79–81], which may allow complete control over the cell sizes and shapes of the bubbles and a more easily maintained liquid fraction of the foam. Silica macroporous scaffolds with vermicular-type mesoporosity were obtained by this air-liquid foaming sol-gel process where nitrogen was bubbled through a mixture of a surfactant and sol-gel precursor [79], while the TiO₂ macrocellular scaffolds obtained had poor mesoporosity arising from the void space induced by the random aggregation of nanoparticles within the foam walls [80]. Macroscopic cell morphologies were tuned by changing the air/liquid:foam ratios and the size of the nitrogen bubbles, while wall topologies were varied by changing the surfactant. Spraying aqueous siliceous solutions containing alkyltrimethylammonium surfactants under high pH conditions

resulted in mesoporous silica foams with hierarchical trimodal pore structures (macrovoids and two kinds of mesopores of around 3 and 40 nm) [81]. The macrocellular structure was produced with air bubbles, which was stabilized through a rapid condensation reaction during drying. The bimodal mesopore distribution was derived from the surfactant micelles and the interparticle spaces of silica nanoparticles (Fig. 10). This hierarchical architecture of the mesoporous silica foams, having extremely low bulk density (0.01 g cm^{-3}), high mesopore volume ($>2 \text{ cm}^3 \text{ g}^{-1}$), and specific surface area ($>1000 \text{ m}^2 \text{ g}^{-1}$), is attributable to the self-assembly of air bubbles, surfactant-siliceous complexes, and mesostructured silicate particles during the spraying, condensation, and drying processes, respectively. However, this method looks complex, and it would be difficult to control all the parameters.

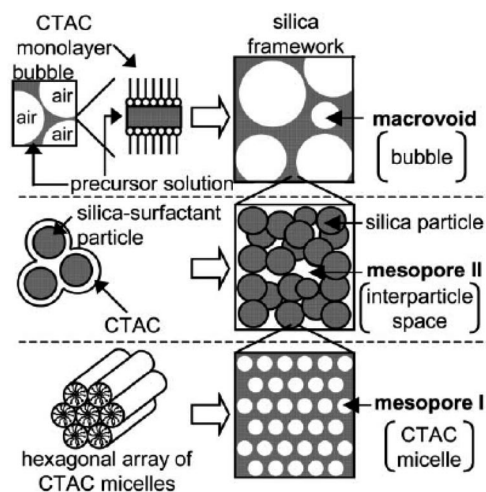


Fig. 10 Schematic model for the hierarchical trimodal pore structure of silica foams by a bubbling process [81].

Preformed polymer foams are also good candidates for templating macroporous structures. Monolithic PS foams, preformed by polymerization of styrene either in the continuous or the dispersed phase of highly concentrated water/oil emulsions, have been used to synthesize meso-/macroporous inorganic oxide monoliths by imbibition of a self-assembling block-copolymer/sol-gel mixture [82]. After calcination to remove the organic components, the resulting meso-/macroporous silica, titania, and zirconia materials retained their macroscopic shapes and possessed independently adjustable meso- and macropore structures. The meso-/macroporous silica monoliths prepared from the W/O PS foams and PEO-PPO-PEO triblock copolymer species consisted of cellular macropores $0.3\text{--}2 \mu\text{m}$ in diameter, interconnected by windows approximately $0.2\text{--}0.5 \mu\text{m}$ in diameter with wall thicknesses of approximately 100 nm , and highly ordered mesopores, 5.1 nm in size. Alternatively, preformed mesoporous silica nanoparticles were used as building blocks to coat polyurethane foam, leading to mineralization of the foam. Subsequent elimination of the organic foam by calcination resulted in monolithic macrocellular silica foams with a trimodal pore system (small mesopores–large mesopores–macropores) [65]. Textural large meso–macropores (in the $20\text{--}70 \text{ nm}$ range) have their origin in the interparticle voids, and the small intraparticle mesopore system ($2\text{--}3 \text{ nm}$ in diameter) owing to the supramolecular templating effect of the surfactant.

SINGLE MICELLE TEMPLATES COMBINED WITH SUPPLEMENTARY CHEMICAL OR PHYSICAL METHODS

Many successful examples have been reported on the preparation of hierarchically porous materials by the combination of a single templating method with a supplementary chemical or physical method, for example, chemical etching, chemical modification, physical deposition, and physical leaching, etc. In some cases, this goal can be simply achieved by the expansion of pore sizes.

Controlled sol-gel processes

A well-documented example is mesoporous silica SBA-15 synthesized by using Pluronic P123 ($\text{EO}_{20}\text{PO}_{70}\text{EO}_{20}$) as the structural directing agent [12–15], which has 2D hexagonal $p6mm$ symmetry and channel-type mesopores. These materials generally have additional micropores in the silica walls resulting from the interpenetrating network of silica and hydrophilic EO chains [85–88]. The micropore volume could be systematically controlled by varying the synthesis temperature and the tetraethyl orthosilicate (TEOS)/surfactant ratio. The result obtained clearly shows that the micropore volume should decrease at elevated synthesis temperatures. Also, an increase in TEOS/surfactant ratio in the starting mixture is found to be an effective method to increase the micropore volume of SBA-15 [89]. The synthesis of plugged hexagonal templated silicas has recently been further developed, in order to optimize the ratio of micro- and mesopores and to improve stability. The materials obtained have a combined micro- and mesoporosity and a tuneable amount of both open and encapsulated mesopores and are much more stable than the other micellar templated structures tested. The high microporous volume and high stability of these plugged hexagonal templated silica materials are governed by internal silica nanocapsules [90].

A single modified triblock copolymer Pluronic P123 (abbreviated P123-COOH) can be used to synthesize mesoporous silica SBA-15 materials with additional meso- or macro intraparticle porosities, depending on the acid concentration in the synthesis mixtures [90]. Carboxylic acids are among the most popular acid catalysts for the control of hydrolysis and condensation of tetraalkoxysilane precursors. When the P123-COOH copolymers form micellar structures in solution, the interfacial monolayer of carboxylate groups may facilitate the hydrolytic condensation of alkoxy silanes during the self-assembly process, resulting in SBA-15 materials with multi-modal and interconnected pore structures (Fig. 11).

Other supplementary chemical or physical methods combined with single templating methods were further developed to synthesize hierarchically porous materials.

Based on the control of sol-gel deposition, a one-pot surfactant-assisted procedure [18] could be used to prepare silica-based materials, both as powders and monoliths. The obtained materials have a bimodal pore system (meso-/large mesoporous or meso-/macroporous) and containing a diversity of dopant elements ($M = \text{Al}, \text{Ti}, \text{V}, \text{Zr}$). Modulation of pore sizes depends on both the surfactant (small pores) and the procedural (synthesis and aging) conditions (large pores). The procedure is based on the use of a simple structural directing agent (CTABr) and a complexing polyalcohol (2,2A,2B-nitrilotriethanol, TEAH₃) able to adequately regulate the rates of the hydrolysis and condensation processes of the different inorganic components (or heteroelements) of the final material. This synthesis strategy has been designed to overcome problems associated with differences in reactivity between the Si source and the other precursor species which contain metal cations. The small mesoporous system is generated with the help of the template effect of the surfactant (it is highly likely that it might be modulated by changing the length of its chains). The large pores (in the border between the meso- and macropore domains) are generated as the nucleation and growth of the primary mesoporous nanoparticles proceeds. Their size can be modulated easily by modifying the water/TEAH₃ ratio in the starting solution, as well as varying the aging time. A simple preparative procedure yielding bimodal porous materials with vari-

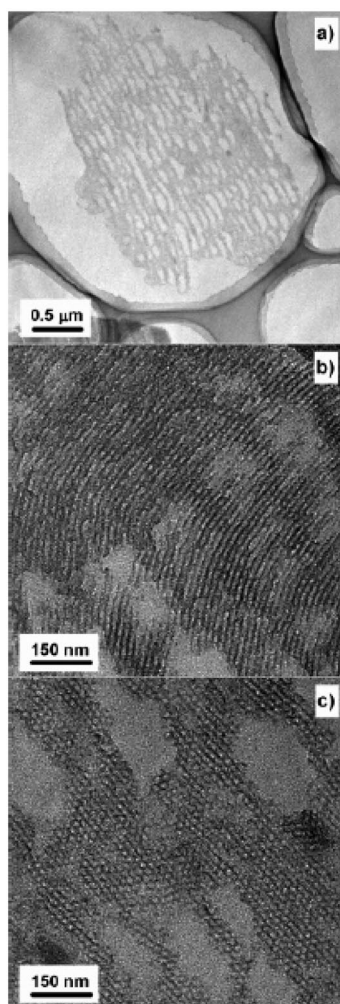


Fig. 11 TEM image of ultramicrotomed mesoporous silica SBA-15 with additionally hierarchically intraparticle porosities [91].

able amounts of different heteroelements was described. The spongy character of these materials results in an enhanced accessibility to their active sites, which confer special interest as possible catalysts.

Similarly, by adding dilute electrolytes in the gel mixture, non-ionically templated [Si]-MSU-X mesoporous silicas with bimodal pore systems in the pore size range 3.0–9.0 nm were synthesized. The results obtained indicate that electrolytes can exert considerable influence over all of the template and silica assembly and condensation processes. The presence of two different mesophases (lamellar and hexagonal) in the network is the origin of the two pore size distributions. The hypothesis is presented that weakly ionic templating systems might provide insights into the interactive roles between weakly ionic biological fluids and hydrogen-bonding templates such as polysaccharides in biomineralization systems. Notably, cations exert structure-directing effects on a proposed flexible PEO/water/silicate ternary complex, leading to modified micelle packing and subsequently modified pore symmetries of materials formed in neutral solutions. Anions, on the other hand, modify the rate and extent of TEOS hydrolysis and condensation through the formation of 5-coordinate intermediates of varying strengths. Fluoride is a special case in that it causes not only greatly increased TEOS condensation and smaller

particle sizes of spherical morphology, but also increased pore diameters. Thus, by adding dilute electrolytes, the sol-gel processes can be modified and controlled to realize the synthesis of bimodal porous silicas.

Phase separation

Chemically induced liquid-liquid phase separation has been applied to the synthesis of siliceous mesoporous materials with co-continuous macropores [92]. This technique is based on the hydrolysis and condensation of inorganic precursors in the aqueous domain of a microphase-separated medium, derived from the self-assembly phase of the template used. A wide variety of water-soluble polymers, such as poly(ethylene oxide), has been used to control the phase separation/gelation kinetics in the preparation of monolithic silica of virtually any shape exhibiting both interconnected macropores and textural mesoporosity. With the use of various Si precursors such as tetramethoxysilane, tetraethoxysilane, and bis(trimethoxysilyl)-ethane, amorphous or disordered mesopores can be embedded in gel networks which constitute a co-continuous macroporous structure [93,94]. The phase separation is driven by the repulsive interaction between the hydrophobic PEO-oligomer complex and the hydrophilic solvent. The macroporous morphology is the result of phase separation that took place earlier than the sol-gel transition. The walls in this macroporous structure consist of aggregates of silica nanoparticles giving rise to textural mesoporosity in the walls with pore sizes in the 10–20 nm range and a high surface area. Poly(ethylene glycol) used together with alkylammonium surfactant was found to give better control over particle aggregation and the internal structure of silica monoliths with hierarchical meso-macroporosity [95], although ordered mesopores were still difficult to obtain. Alkoxide-derived alumina-silica [96] and silica-zirconia [97] having meso-/macroporous structure can also be synthesized by this technique in the presence of polyethylene oxide, however, the formation of a 3D interconnected macroporous structure was seldom achieved in transition-metal alkoxide-derived sol-gel systems [98]. This is because the transition-metal alkoxides are very reactive toward hydrolysis, and it is generally difficult to control the structural development until gelation. Monolithic macro-/mesoporous ethanesilica [99] and pure silica [100] gels have also been synthesized via polymerization-induced phase separation in the presence of the BC P123 and a micelle-swelling agent 1,3,5-trimethylbenzene.

The addition of a micelle-swelling agent was found to induce the mesostructural transformation from 2D hexagonally ordered to mesostructured cellular foam, accompanied by minor modifications or even without disturbing the macroporous framework structure. The orderliness of the mesostructures was confirmed by field emission-scanning electron microscopy (FE-SEM) and X-ray diffraction (XRD). Whereas, Shi et al. [101] synthesized the silica monolith with textural pores and ordered mesopores, similar to the ethanesilica-based monolith reported by Nakanishi et al. [99,100], by a sol-gel process using the triblock polymer F127 as a pore directing reagent, where F127 demonstrated its dual functions of phase separation and meso-templating. They found that the ordered hexagonal mesopores in the silica skeletons, observed in TEM images but not supported by XRD patterns, were not connected. Considering that short-chain alcohols generated by the hydrolysis reaction of metal alkoxides generally disturb the self-organization of structure-directing agents, leading to the disordering of the mesostructures of the product, several efforts have been devoted to organizing a highly ordered mesoporous gel network into macroporous assemblies. The undesired co-presence of short-chain alcohol molecules in the mesostructure-forming stage could be avoided by modification of the starting alkoxide, and thus hierarchical porous silica networks, built up from periodic interconnected mesoporous silica strands, was synthesized (Fig. 12) [102,103]. Using ethylene glycol and propane-1,2-diol-modified silanes as inorganic precursors and an amphiphilic triblock copolymer as a structure-directing agent [104], silica monoliths exhibiting a unique hierarchical network structure with a bimodal pore size distribution in the macro- and mesopore size regime with high surface areas were prepared by phase separation on different levels. In addition to an extraordinary cellular network structure with interconnected macropores, several hundreds of nanometers in diameter, the material exhibits a well-ordered

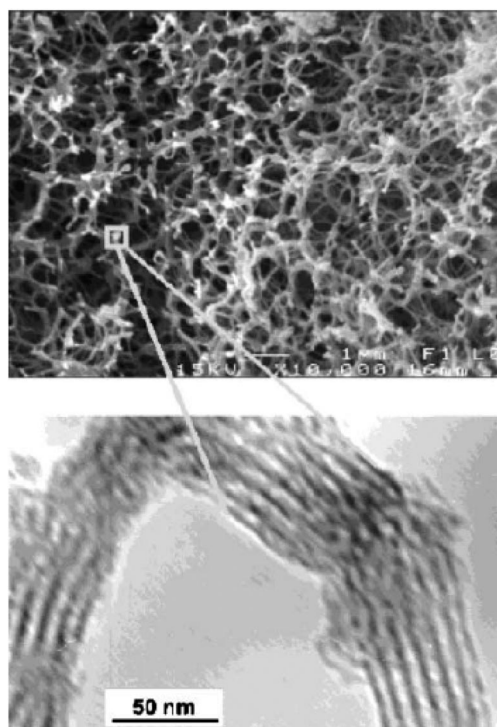


Fig. 12 SEM (top) and TEM (bottom) of a macro-/mesoporous silica monolith synthesized with ethylene glycol-modified silane as an inorganic precursor and the triblock copolymer P123 as a meso-template [102].

mesostructure with periodically arranged mesopores of about 6–10 nm in diameter. However, the use of glycerol-modified silanes resulted in the formation of a disordered silica mesostructure. The modified silane can offer two major advantages compared to the conventionally used TEOS and tetramethoxysilanes: the precursor is water-soluble and thus allows a direct mixing with the lyotropic liquid-crystal-like phase of the BC in water; second, it does not require a catalyst to start the hydrolysis and condensation reactions [102]. The ethylene glycol, released during the hydrolysis and condensation reactions, is not detrimental to most of the liquid-crystal surfactant mesophases.

Post-treatments

Post-treatments, such as chemical etching or postsynthesis, have also been successfully exploited in the preparation of hierarchically porous materials [14]. Primarily, the MCM-41 mesoporous materials were treated in a solution of NH_4OH , this chemical etching process resulted in the formation of bimodal mesoporous materials. The pore structure characteristics were affected by the treatment temperature and time. Ammonia should play an important role in such a pore expansion process. Due to the volatility of ammonia, ammonia molecules should penetrate inside the nanochannels more easily than water, and thus the swelled channels lead to the pore size expansion from 2.3 to about 4 nm. Since the thermal stability of surfactant CPCI is low (melting point of 86 °C), part of the surfactant species in the mesochannels may start to decompose after hydrothermal treatment for three days. Some neutral, solubilizing species, such as pyridium, may be formed which may result in degradation of part of the channels. Also, since some surfactant molecules would be leached out during hydrothermal treatment, the silica walls would tend to collapse inward, making the mesochannels interconnected. The porosity of these

two types of mesopores can be controlled by varying the treatment time as well as the concentration of ammonia.

Compared to chemical etching of the silica walls of the primary porous materials, the postsynthesis method is as an efficient route to include additional porous structures into the primary porous materials. Various types of hierarchically porous nanostructures have been explored from compositions such as inorganic materials, polymers, and carbon, and composites for the porous supports [105–128].

First, ordered porous cores such as spherically mesoporous materials and microporous zeolites have successfully been used to synthesize core-shell structures, obtaining mesoporous/polymer/zeolites and zeolites/polymer/mesoporous samples [116–128].

The generally synthetic procedure is shown in Fig. 13 [125]. Porous particles (zeolites) were taken as the core materials, with a mesoporous shell layer, fabricated by cohydrolysis and subsequent sol-gel condensation of TEOS and organic template micelles, coated onto each core particle. Then the bimodal porous silicate with a zeolite core/mesoporous shell (ZCMS) structure was formed. In this case, the shells have a 3D interconnected randomly distributed mesopore arrangement which renders the precise control of this novel structure possible. It is very interesting that the fabrication of carbon and silica nanocases with hierarchical structures could subsequently be synthesized by employing the ZCMS silicate as a template.

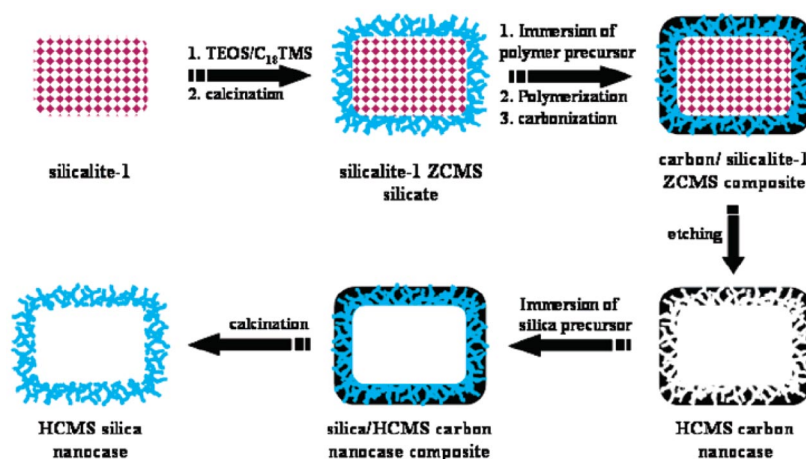


Fig. 13 Schematic illustration for synthesis of silicalite-1 zeolite core/mesoporous shell (ZCMS) particles and corresponding pseudohexagonal prismatic hollow core/mesoporous shell (HCMS) carbon and silica nanocases [125].

Secondly, the wall of mesoporous silicates could be coated or doped with zeolite nanocrystals, which create valence bonds with the mesoporous supports, consequently imparting microporosity [129–138]. The introduction of zeolite seeds into the wall of nanoporous aluminosilicates is also a simple and general means of improving hydrothermal stability and acidity. Unit cells of ZSM-5 were introduced into mesoporous materials by ion exchange of the nanoporous aluminosilicates with the tetrapropylammonium cation (TPA) as an MFI structure-directing agent and then digestion of the mesoporous materials in glycerol [137,138]. This led to the formation of a mesostructured zeolite phase. Pinnavaia and co-workers [129–131] and Xiao et al. [132–134] also reported steam stable aluminosilicate mesostructures assembled from zeolite-type seeds. In the latter cases, the XRD patterns did not show crystalline features. Evidence for the presence of zeolite unit cells may, however, be provided by nitrogen adsorption and desorption isotherms and the acid catalytic activity of such materials [129–134]. A new synthetic method was developed to synthesize a mesoporous material with semi-

crystalline zeolitic walls. This procedure, called zeolite-coated, involves a templated solid-state secondary crystallization of zeolites, starting from the amorphous mesoporous materials of corresponding elemental composition. It is important that the walls of the amorphous mesoporous precursor material are as thick as possible [135,136]. The seed-introduced products exhibited well-defined small-angle XRD patterns, which were characteristic of an ordered mesoporous material. However, these materials did not exhibit the long-range atomic order characteristic of a crystalline zeolite framework, and the properties were still far from those of crystalline zeolites [139], therefore being insufficient for many industrial applications. Hierarchical zeolites are a hot research topic at the moment due to their strong industrial promise. Materials scientists endeavor to design and develop rational synthesis pathways for microporous zeolites with hierarchically porous structures. Here we present a feature section of zeolites with hierarchically porous structures.

Template-directed depositions and chemically induced transformation methods for the fabrication of hollow inorganic microspheres

In recent years, inorganic hollow nanostructures with defined structure, composition, and tailored properties have attracted more and more attention because of their potential applications for the controlled release of various substances, catalysis, drug delivery, protection of environmentally sensitive biological molecules, lightweight filler materials, and chemical reactors [140–146]. Among various preparation methods, the template-directed synthetic method has been proved to be the most effective route for preparing hollow microspheres. The template methods often involve the coating of nanocrystals on the template surface, followed by removal of the template using calcination or etching. These post-treatment processing steps are costly, wasteful, and of environmental concern and thus limit the application of the template-directed approach. Clearly, these problems will be easily solved if inorganic hollow nanostructures could be prepared by a facile self-transformation route. Yu et al. [140] reported a simple one-step template method for the fabrication of crystalline titania (TiO_2) hollow microspheres, based on template-directed deposition and in situ template-sacrificial dissolution. The prepared TiO_2 hollow spheres exhibit hierarchically nanoporous structures on a multilength scale (from micropores, mesopores, large-mesopores to macropores) (Fig. 14) and a high photocatalytic activity. Photoactive ZnO hollow spheres with porous crystalline shells were one-pot fabricated by hydrothermal treatment of glucose/ ZnCl_2 mixtures at 180 °C for 24 h, and then calcined at different temperatures for 4 h [141]. Further results show that hollow spheres can be more readily separated from the slurry system by filtration or sedimentation after the photocatalytic reaction and reused than a conventional powder photocatalyst. In 2006, Yu and Mann [142–146] proposed a chemically induced self-transformation (CIST) method used to construct hollow inorganic microspheres with complex internal and external textures. Two contrasting approaches, involving either polymer- or fluoride-mediated transformation of amorphous solid particles, were reported as general routes to the fabrication of hollow inorganic microspheres. Firstly, calcium carbonate (Fig. 15) and strontium tungstate hollow microspheres were fabricated in high yield using sodium poly(4-styrenesulfonate) as a stabilizing agent. Secondly, the fabrication process was extended to relatively stable amorphous microspheres, such as TiO_2 and SnO_2 , by increasing the surface reactivity of the solid precursor particles using fluoride ions as promoters to produce well-defined hollow spheroids of nanocrystalline TiO_2 and SnO_2 . In each case, the hollow microspheres, which were composed of polycrystalline walls of aggregated nanoparticles, were produced in high yield and exhibit good reproducibility. Furthermore, Mann and Yu [143] reported the preparation of polycrystalline $\text{WO}_3 \cdot 1/3\text{H}_2\text{O}$ hollow microspheres with hierarchically porous wall structures and detached internal amorphous cores in close to 100 % yield using the CIST method (Fig. 16). These prepared hollow superstructures (including $\text{WO}_3 \cdot 1/3\text{H}_2\text{O}$, $\text{CuO}/\text{Cu}_2\text{O}$, and TiO_2) usually exhibit a significant photocatalytic activity [145].

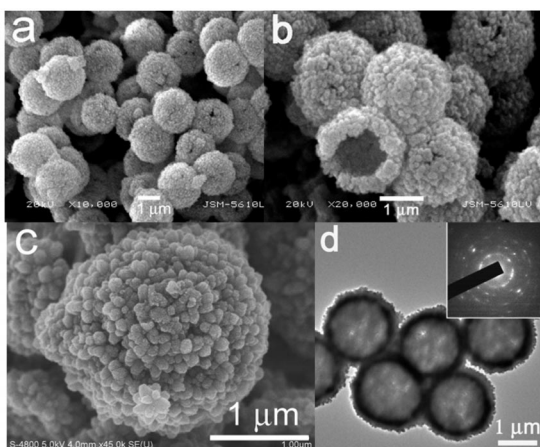


Fig. 14 SEM (a and b), FE-SEM (c), and TEM (d) images of TiO_2 hollow spheres obtained in a 0.02 M TiF_4 aqueous solution at 60 °C for 12 h. Inset in (d) shows the selected area electron diffraction (SAED) pattern of individual [140].

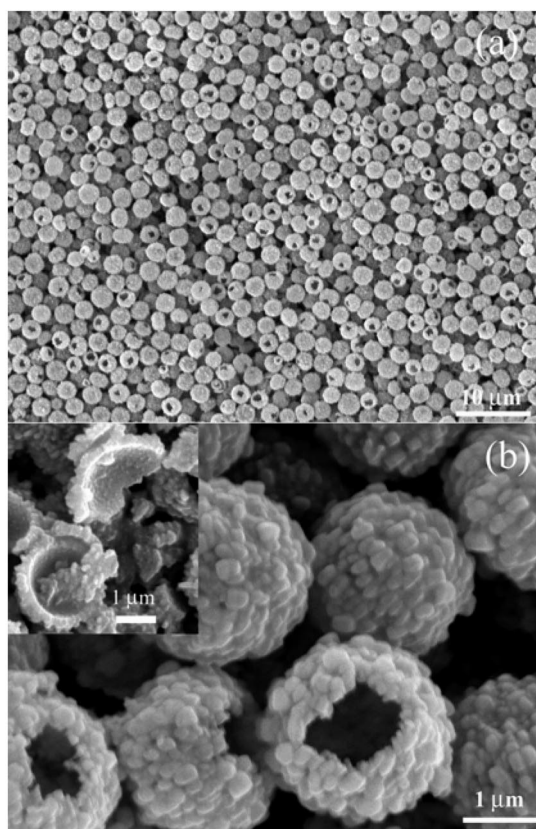


Fig. 15 (a) Low- and (b) high-magnification SEM images of calcium carbonate hollow microspheres prepared at 70 °C and pH = 10.5 in the presence of 1.0 g l^{-1} PSS and $[\text{CaCO}_3] = 8 \text{ mM}$. Inset in (b) shows magnified image of fractured spheres showing smooth and rough inner and outer surfaces, respectively [142].

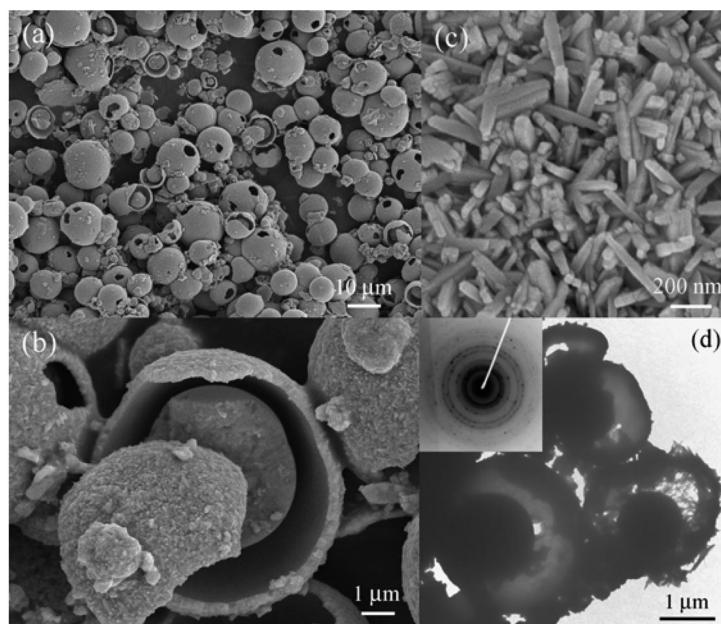


Fig. 16 (a) Low- and (b) high-magnification SEM images of $\text{WO}_3 \cdot 1/3\text{H}_2\text{O}$ hollow microspheres prepared at 80°C in the presence of 0.2 g l^{-1} PSS and 4 ml HNO_3 after ripening for 20 h. The presence of both a detached core and intact external shell are shown in (b). (c) High-magnification SEM image of the external surface of the shell of a hollow microsphere showing aggregated rod-like particles and associated porosity. (d) TEM image showing detached cores and shells of three hollow microspheres. Inset in (d) shows electron diffraction pattern for polycrystalline $\text{WO}_3 \cdot 1/3\text{H}_2\text{O}$ [143].

TEMPLATED SYNTHESIS OF HIERARCHICALLY POROUS MATERIALS WITH FEATURED CHEMICAL COMPOSITIONS

Controlled phase-separation in the synthesis of zeolites with hierarchically porous structures

Zeolites are crystalline, hydrated aluminosilicates with open 3D structures built of $[\text{SiO}_4]^-$ and $[\text{AlO}_4]^-$ tetrahedra linked to each other by sharing all the oxygens to form regular intracrystalline cavities and channels of molecular dimensions. These materials are very strongly hydrothermally and thermally stable, and are of considerable technological importance as shape-selective catalysts, ion-exchange solids, and molecular sieves. However, despite all the catalytically desirable properties of zeolites, their small microporous channels are subject to diffusional limitations that restrict accessibility to their internal surfaces. Introducing mesopores or macropores linked to the zeolitic micropores, so as to increase accessibility to the internal surface, has been investigated in an effort to extend the application of zeolites to the treatment of large molecules.

Compared to supramolecular and bulky aggregation templates, small molecular templates for zeolites (e.g., tetrapropylammonium and alkali metal ions) tend to separately form zeolite structures, even presenting other templates such as supramolecular templates. Research has shown that the two different templating systems worked in a competitive, rather than a cooperative, manner. The syntheses mostly resulted in the formation of an amorphous mesoporous material, bulk zeolite without mesoporosity, or a physical mixture of two phases [147–150]. The traditional methods, such as steaming, leaching (acid or base), or chemical treatment [94], could be used to increase mesopores or macropores

of synthesized zeolites, however, the pore amount, type, and size are not easy to control due to the complexity in the synthesis and limitation of various synthetic routes. Multistep synthesis strategies were proposed to solve the phase-separation problem of the zeolite and other porous phases.

Recently, it was also reported that mesoporous materials with crystalline zeolite frameworks can be synthesized through a crystallization process inside a packed bed of removable “solid” nanotemplates (e.g., carbon nanoparticles [151–153], nanotubes [154], mesoporous carbons [155], polymer beads [35], and other materials [156]). ZSM-5 with mesopores of diameter 5–50 nm has been synthesized by growing the zeolite crystals in the pore system of carbon black [151,152]. Pinnavaia and co-workers, on the other hand, prepared ZSM-5 with large mesopores (typical pore size larger than 10 nm) using colloid-imprinted carbons as the template [153]. Kaneko and co-workers have synthesized mesoporous ZAM-5 with secondary mesopores with a diameter of 11 nm using carbon aerogel as the template [154]. Holland et al. [35] used a dual-templating route for the formation of macroporous (pore size ca. 250 nm) silicalite with zeolitic frameworks while Dong et al. [156] prepared zeolite monoliths with large macropores (up to 1.5 μm in diameter) using spherically mesoporous silica. In all these studies [35,152–156], the pore channels introduced were invariably large (i.e., in the upper meso- to macropore range). The synthesis approaches were based on the idea that the small solid particle templates could be removed to introduce additionally porous structures within zeolites. This is a nice and elegant idea, but the concept of synthesis is in essence the same as the dual and multiple template synthesis of hierarchically porous materials mentioned above, and the process using a solid template has limited pore tunability depending on the availability of templates.

As mentioned above, crystalline zeolite containing both micro- and mesoporous structures in a single phase is still difficult to obtain if the aluminosilicate gel is directly crystallized in the presence of ordinary organic surfactants and molecular templates for zeolites. The phase-separation phenomenon indicates that the surfactants are expelled from the aluminosilicate domain during the zeolite crystallization process, making it difficult for the surfactants to modulate the zeolite crystal growth into a mesoporous structure. Tremendous progress has been made in the one-step hydrothermal synthesis of hierarchical mesoporous zeolites, templated from a mixture of small organic ammonium salts and mesoscale cationic polymers by Xiao et al. [157]. Hierarchical mesoporous β -zeolite was crystallized in the presence of TEOH and a mesoscale cationic polymer, polydiallyldimethylammonium chloride (PDADMAC). The presence of hierarchical mesoporosity in the mesoporous β -zeolite sample is attributed to the use of the molecular and aggregated cationic polymer PDADMAC. The cationic polymers could effectively interact with negatively charged inorganic silica species in alkaline media, resulting in the hierarchical mesoporosity.

Further, a direct synthesis route was also developed by Ryoo et al. [158] to synthesize mesoporous zeolites using amphiphilic organosilanes as a mesopore-directing agent. The mesopore diameters of the product can be finely tuned, typically in the range of 2–20 nm, depending on the molecular structure of the mesopore-directing silanes and the hydrothermal synthesis conditions, which is very desirable and important for application in shape-selective catalysts, ion-exchange solids, and molecular sieves. The key for the synthesis was to design amphiphilic surfactant molecules that contained a hydrolyzable methoxysilyl moiety, a zeolite structure-directing group such as quaternary ammonium, and a hydrophobic alkyl chain moiety. It was expected that such amphiphilic organosilanes could strongly interact with growing crystal domains through the formation of covalent bonds with other SiO_2 and Al_2O_3 sources using the methoxysilyl moiety. [3-(trimethoxysilyl)propyl]hexadecyldimethylammonium chloride ($[(\text{CH}_3\text{O})_3\text{SiC}_3\text{H}_6\text{N}(\text{CH}_3)_2\text{C}_{16}\text{H}_{33}]\text{Cl}$, TPHAC) was used in this case, which contains a surfactant-like long-chain alkylammonium moiety and a hydrolyzable methoxysilyl group, linked together by a Si–C bond. The organic molecules that are capable of a strong interaction with the growing crystal surface can effectively modulate the crystallization process of inorganic materials. In this strategy, globular MFI zeolite particles had a highly mesoporous structure, as indicated by high-resolution SEM and TEM images (Fig. 17). Moreover, the formation of the mesoporous zeolite particles was well supported by a small-angle XRD peak appearing at 0.7° and the wide-angle XRD peaks corresponding

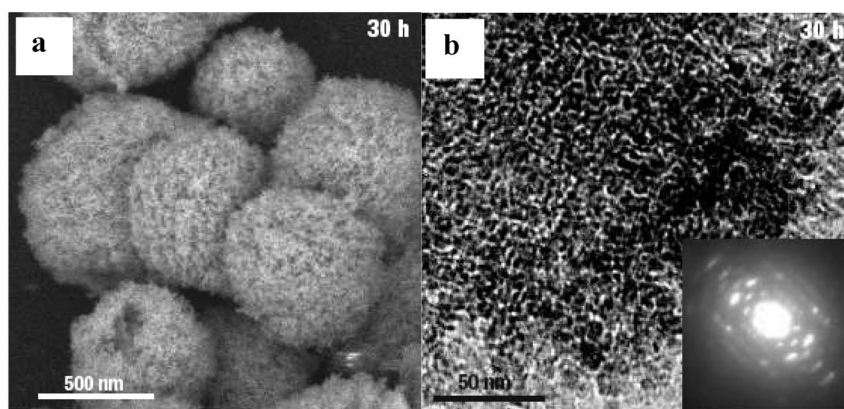


Fig. 17 SEM (a) and TEM (b) images of mesoporous MFI zeolite synthesized using the amphiphilic organosilanes [158].

to the MFI zeolite structure. Crystalline zeolites with both mesoporosity and strong acidity may bridge the gap between conventional bulk zeolite and amorphous mesoporous aluminosilicates, particularly for catalytic applications involving large molecules. Furthermore, the controlled phase-separation synthesis principles developed may be applied to other hierarchically structured materials.

Template replication in synthesis of carbons with hierarchically porous structure

Porous carbon materials have received a great deal of attention due to the myriad of applications [159,160]. Many kinds of rigid and specially designed inorganic templates have been employed in an attempt to synthesize carbons with uniform pore sizes. Knox and his co-workers pioneered the template synthesis of porous carbons [161]. The general template synthetic procedure or template replication procedure for porous carbons is as follows: (1) preparation of the carbon precursor/inorganic template composite, (2) carbonization, and (3) removal of the inorganic template. Broadly speaking, the template approaches can be classified into two categories. In the first approach, inorganic templates such as silica nanoparticles are embedded in the carbon precursor. Carbonization followed by the removal of the template generates porous carbon materials with isolated pores that are occupied by the template species. In the second approach, a carbon precursor is introduced into the pores of the template. Carbonization and the subsequent removal of the templates generate porous carbons with interconnected pore structures.

Based on this template replication strategy, the mesoporous carbons, having hierarchical structures, were synthesized using hierarchically ordered mesoporous silica (meso-nano-S) materials as templates [162]. It was important to control the amount of carbon precursor, such that it would be selectively incorporated into the framework pores of the bimodal silica template. The carbon precursor, phenol, was first adsorbed into the small pores because capillary condensation into small pores occurs at low pressure. The meso-nano-C carbon so produced was composed of 30–50-nm-sized particles having 3D wormhole-like pores, and was the exact negative replica of the meso-nano-S silica template. Similarly, co-imprinting of hexagonally ordered SBA-15 particles and 13-nm-sized colloidal silica particles in pitch followed by carbonization and removal of the silica templates can generate bimodal mesoporous carbons [163]. Using a corresponding template, various hierarchically porous carbons were also successfully replicated, for example, hierarchical mesocellular mesoporous carbon foam [164], hierarchically porous monolithic carbon containing wormhole-like mesopores and macropores [165], HCMS carbon [125,166,167], mesoporous carbon rods [168], and spherical-shaped mesoporous carbon [169]. The pore size of the resulting macroporous carbon materials could be easily controlled by vary-

ing the particle size of the silica spheres. Various macroporous carbon materials were synthesized using synthetic silica opals, which were made by using colloidal crystals, self-assembled uniform-sized silica spheres, as templates [170–174]. The removal of the silica template generated macroporous carbons with inverse opal structures.

In further cases, Yu and Jaroniec reported the preparation of ordered nanoporous carbons with hierarchically highly graphitized structures using commercial mesophase pitch as a carbon precursor and silica colloidal crystals as templates [175]. Interconnected, ordered spherical pores and relatively large graphite crystallites (interlayer spacing of ca. 0.33 nm) in the carbon pore walls were clearly observed in the TEM image. The replication of meso-/macroporous silica enables the preparation of hierarchical bimodal porous carbon with various shapes, where the macroscopic shape can be controlled through the shape of the silica monolith used as the template structure, and the macropore diameter can be varied between 0.5–30 μm in a controlled manner [165,176,177]. The carbon monolith is a positive replica of the silica monolith on the micrometer scale, but a negative replica on the nanometer scale. Linden and co-workers [165,176] reported the hierarchical carbon replica of their meso-/macroporous silica [97], and the meso-/macroporous carbon had a BET surface area of over 1000 $\text{m}^2 \text{g}^{-1}$ and a specific pore volume of 1.2 $\text{cm}^3 \text{g}^{-1}$. A significant microporosity can be obtained in these carbon replicas, leading to the trimodal porous carbons [176,177]. Ordered macroporous carbon with mesoporous walls has also been produced by the template replication of aggregates of small silica particles, which were themselves templated by a self-assembled lattice of larger monodisperse polystyrene spheres [178]. Figure 18a shows the SEM images of the silica template composed of silica nanoparticles of about 12 nm in size forming the walls of macropores of about 330 nm in diameter. The voids between the packed silica nanoparticles provide fully interconnected mesopores, which can be impregnated with the carbon precursor divinylbenzene. The carbonization of the carbon precursor and subsequent dissolution of the silica particle framework resulted in a bimodal porous carbon replica composed of macropores of about 317 nm in diameter connected to small mesopores of about 10 nm in size (Fig. 18b). Three

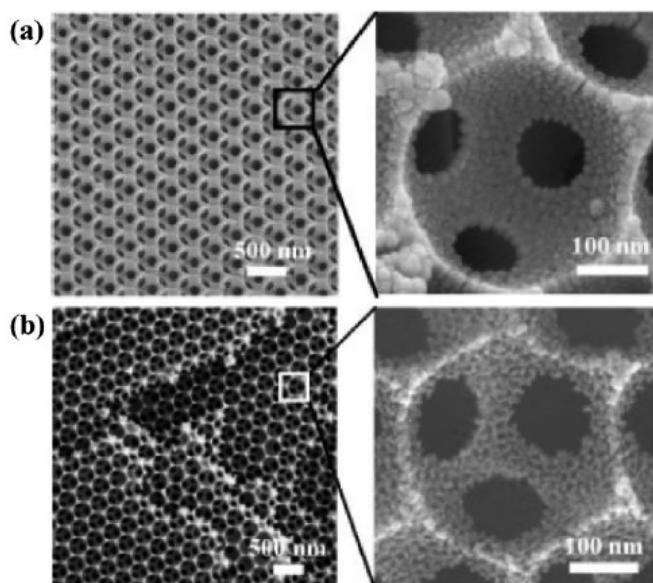


Fig. 18 SEM images at different magnifications of a silica template composed of (a) silica nanoparticles of about 12 nm in size forming the wall of macropores of about 330 nm in diameter, and (b) the resulting bimodal porous carbon replica composed of macropores of about 317 nm in diameter connected to small mesopores of about 10 nm in size. This periodically ordered, bimodal porous carbon is termed POBPC(317-10) [178].

round holes in the wall appear as black dots with diameters of about 110 nm, through which a macropore is connected to the three neighboring macropores below the macropore in the image. The size of the large macropores can be manipulated by controlling the diameter of the PS spheres, while the size of the small mesopores and the overall specific surface area are determined by the silica nanoparticles. However, this interconnected, ordered, uniform pore structure in carbon has a relatively low BET surface area of $465 \text{ m}^2 \text{ g}^{-1}$ with total pore volume of $1.32 \text{ cm}^3 \text{ g}^{-1}$, in comparison to the silica template ($>1000 \text{ m}^2 \text{ g}^{-1}$).

Most importantly, the template replication principles have been widely developed to synthesize other hierarchically structured materials including novel structures and inorganic oxides [95,179–184]. For example, freestanding macroporous nickel films were formed as a replica of the macroporous silicon skeleton [182] and the resultant nickel skeleton was punctured by nanopores, making the surface area of the nickel film much larger than that of the starting macroporous silicon. The fabrication of hierarchical tube-in-tube carbon nanotubes is also formed using an anodic aluminum oxide (AAO) film template [183]. An array of mesoporous silica microrods prepared inside macroporous silicon templates with perfluorated pore walls can easily be pulled out of the pores [184].

SELF-FORMATION PROCEDURE AND POROGEN CONCEPT

“Porogen” in synthesis of meso-/macroporous structure

On the basis of a large series of comprehensive studies [14,75,185–201], we found that hierarchical meso-/macroporous metal oxides can be synthesized even without the need for any macrotemplates such as small solid particles, liquid drops, air bubbles, or supplementary chemical and physical methods, by a “one-pot” self-formation process [185–199]. The initial work was done on zirconia [186,187], alumina [188,202], titania, and binary mixed oxides [189,190] via the hydrolysis of the corresponding metal alkoxides in the presence of a single surfactant (either cationic or non-ionic surfactant). The synthesized materials exhibit a parallel-arrayed channel-like macroporous structure, generally having a dense layer on the face of the monolithic particles at the end of the macrochannels [185–187,200,201] (Fig. 19). The macroporous framework is composed of accessible mesopores with a wormhole-like array. The framework walls of aluminum oxides can even be crystalline with boehmite and γ -alumina phases, and their mesostructures were formed through the scaffold-like aggregation and intergrowth of the boehmite and γ -alumina nanofibers, respectively [188]. Such a macromorphology is distinct from the materials obtained by the use of macrotemplates (small solid particles, liquid drops, air bubbles) or supplementary chemical and physical methods. The preliminary studies suggested that the single surfactant would direct the formation of inorganic phases with multidimensional pore systems by the formation of vesicle-type supermicelles resulting from the aggregation of unreacted excess surfactants [186].

The hydrolysis/polycondensation of aluminum sec-butoxide in a mixed solution of H_3PO_4 and Na_2HPO_4 led to the formation of hierarchically phosphated meso-/macroporous nanocrystalline aluminum (oxyhydr)oxides, which incorporated phosphorus into the framework by the surface Al–O–P bonding using surfactant Brij56 [191]. A previous study found that surfactant molecules take no direct role in the formation of either meso- or macroporous structures but significantly influence the textural properties and porosities of the resultant phosphated aluminum (oxyhydr)oxides which possessed high thermal stability, high surface areas, and large acidity.

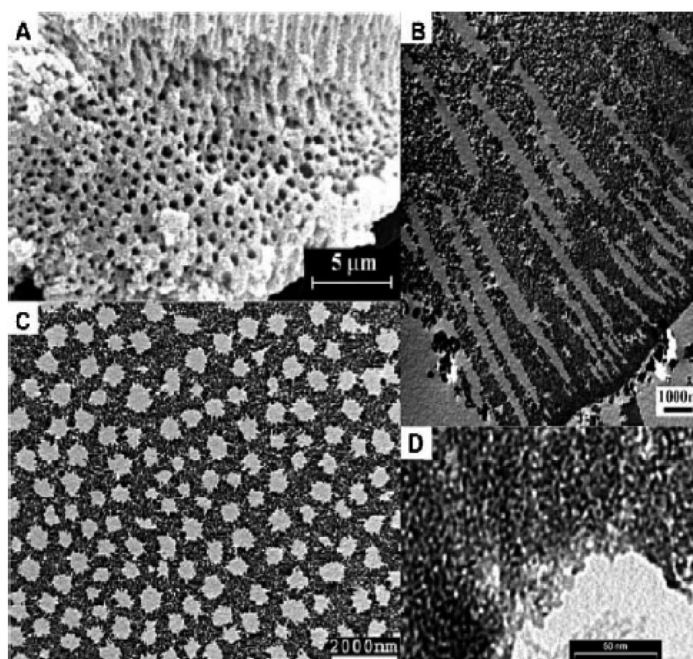


Fig. 19 (A) SEM and (B–D) cross-sectional TEM images of the meso-/macroporous zirconia synthesized with one single surfactant, viewing from different directions and with different magnifications [185].

Hierarchically meso-/macroporous titanium phosphate, obtained by direct hydrolysis of titanium tetrapropoxide in an aqueous orthophosphoric acid solution, demonstrated a macroporous structure of 50–160 nm in size with mesoporous walls (Fig. 20a) [192]. The addition of a small quantity of non-ionic poly(ethylene) oxide surfactant (e.g., 5 %) led to an improvement in the macroporosity with a slight enlargement of macropore sizes to 80–250 nm (Fig. 20b). A secondary large macropore system with parallel channels of 500–1000 nm in size was obtained when the synthesis was performed with 10 % surfactant content, leading to the bimodal macroporous structure with mesoporous walls (Fig. 20c). Further increase in surfactant quantity resulted in the presence of a uniform 3D co-continuous macroporous structure with accessible wormhole-like mesoporous walls (Fig. 20d). This new series of experiments again highlights the hot discussion on the role of the surfactant molecules during the formation of hierarchical porosity. The precise mechanism underlying these hierarchical materials remains elusive. It is interesting to note that the macrochannel shapes (funnel-like or straight tubular) could be tunable, depending on the synthesis conditions and inorganic source used [185–200]. Since then, this new field becomes quite active and attracts particular interest from academia and industry.

Chen et al. [203] synthesized thermally stable meso-/macroporous zirconia with a nanocrystallized framework by using composite surfactants of the amphiphilic BC P123 and poly(ethylene) oxide surfactant Brij56 at a hydrothermal treatment temperature of 130 °C which is considerably higher than the generally reported 60–80 °C [186,187]. The big hydrophobic cores of P123 can adsorb a great number of small-sized hydrophobic groups of Brij56 surfactant molecules. The surplus composite surfactant micelles can aggregate by self-assembly to form “supermicelles” and adsorb onto the hydrophilic solid surfaces, directing the formation of macroporous structures of mesostructured zirconia. Since higher temperatures do not favor the formation of surfactant supermicelles, few macroporous structures were obtained when one single surfactant was used at this elevated temperature. The use of the amphiphilic BC (P123) was believed to be responsible for the improved ordering of the pore structures and the crystallization of the framework without pore structure collapse via certain cooperative effects with

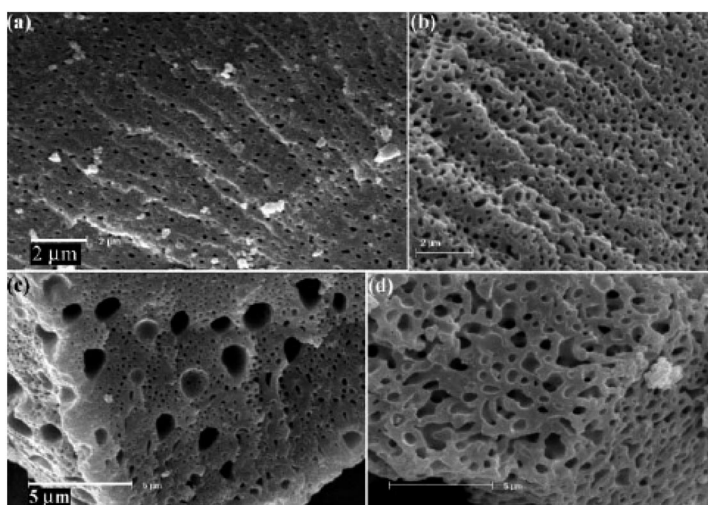


Fig. 20 SEM images of the meso-/macroporous titanium phosphates synthesized (a) in the absence of surfactant, and in the presence of (b) 5 %, (c) 10 %, and (d) 15 % surfactant Brij 56 [192].

the small-sized Brij56 surfactant molecules. This result does support the initially proposed formation mechanism [186,187]. However, the application of this method to silica was not successful [200], which may be the effect of the fast hydrolysis rate of the metal alkoxides. Thus, further work is really necessary to reveal the true mechanism of this spontaneous formation process of meso-/macroporous materials.

Recent reports have also revealed that similar macroporous structures could be spontaneously formed even in the absence of surfactants [193,195–197,199,204,205], although the formation of the macropores required the presence of an alkoxide droplet within the synthesis mixture. The surfactant played no role other than to influence the hydrodynamic conditions during synthesis [205], which could influence the texture of the final materials, since the macropore-free layer was observed on one side of the particle coupled with the curvature of the particle. This self-formation phenomenon of porous hierarchy can be applied to synthesize a large series of transition-metal oxides with hierarchically organized meso-/macroporosity in one solid body. Very pure oxide materials can be prepared starting with just the alkoxide precursors in aqueous solution, as opposed to other synthesis strategies where resultant oxides are often contaminated by residual species.

Mann and co-workers [204] proposed a formation mechanism involving the initial formation of a semipermeable membrane on the outside of the alkoxide droplet, which restricted the hydrolysis/condensation domain such that the reaction subsequently moved inward. The formation of the macropore channels was attributed to microphase-separated regions of metal oxide and solvent established by the flow of the solvent across the membrane to the alkoxide interface. Once the macropore channels were formed, they would preferentially propagate toward the alkoxide since it would provide the least resistant path for the water to react at the solution/alkoxide interface. Although this proposed formation mechanism could explain many of the observations, it still appears to leave several outstanding questions [205]. For example, the mean macropore size distribution increased with the solvent Reynolds number [148], and tubular macrochannels with open tips were often seen in similar particle synthesis (Fig. 21) [189,191,193–195,201].

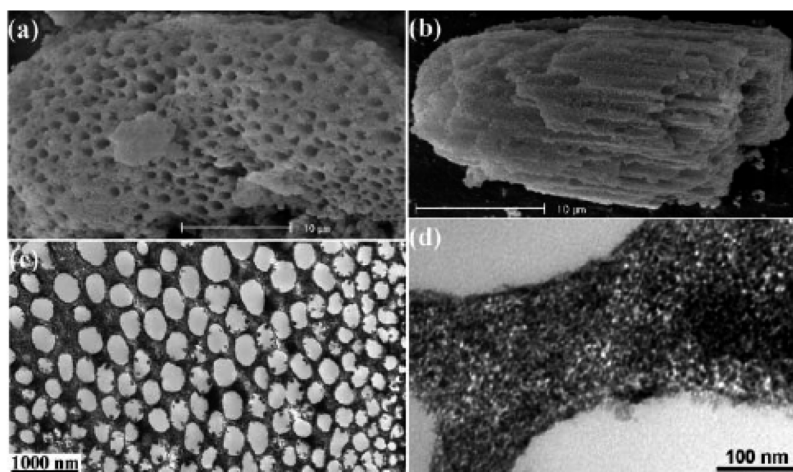


Fig. 21 (a, b) SEM images and (c, d) cross-sectional TEM images of hierarchically macroporous zirconium phosphate with supermicroporous walls spontaneously formed in the absence of surfactant [193].

Very recently, following a series of works [193,195–197,199], Yu et al. [206] also reported the fabrication of hierarchically macro-/mesoporous TiO_2 photocatalytic materials in pure water without using templates and additives at room temperature. At 300 °C, the calcined sample showed very high photocatalytic activity for the photocatalytic oxidative decomposition of acetone in air due to its high specific surface areas and hierarchical macro-/mesoporous structures, furthermore its photocatalytic activity was more than two times higher than that of commercial-grade Degussa P25 TiO_2 powder (P25), which is well known for its superior photocatalytic activity. Moreover, the calcined samples showed especially high thermal stability and the macroporous channel structures were even preserved after calcination at 800 °C (Fig. 22), although the mesostructure was damaged because of the phase transformation from anatase to rutile and sintering. Furthermore, Yu et al. [207] reported the preparation and enhanced photocatalytic activity of trimodally sponge-like macro-/mesoporous titania (Fig. 23) by a hydrothermal treatment of the precipitates of tetrabutyl titanate $[\text{Ti}(\text{OC}_4\text{H}_9)_4]$ in pure water without using any templates or additives. All TiO_2 powders hydrothermally treated at 180 °C showed trimodal pore-size distributions in the macro-/mesoporous region: fine intraparticle mesopores with peak pore diameters of ca. 3.7–6.9 nm, larger interparticle mesopores with peak pore diameters of ca. 23–39 nm, and macropores with pore diameter of ca. 0.5–3 μm . The hierarchically porous titania powders prepared at 180 °C for 24 h displayed an excellent photocatalytic activity, probably due to their special pore wall structure. Their photocatalytic activity was 3 times higher than that of P25. This novel trimodal macro-/mesostructured titania should also find potential applications in numerous fields including photocatalysis, catalysis, solar cells, separation and purification processes, and so on because the textural mesopores and intrinsic interconnected pore systems of macrostructures should efficiently transport guest species and light to framework binding sites.

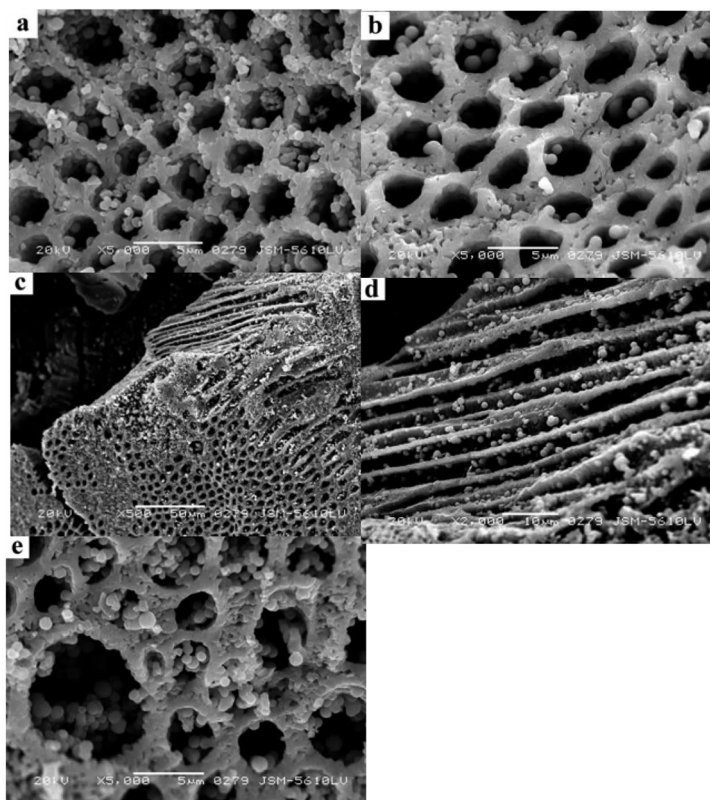


Fig. 22 SEM images of the as-prepared (a) and calcined hierarchical macro-/mesoporous TiO_2 samples at (b) 300 °C, (c and d) 500 °C and (e) 800 °C [206].

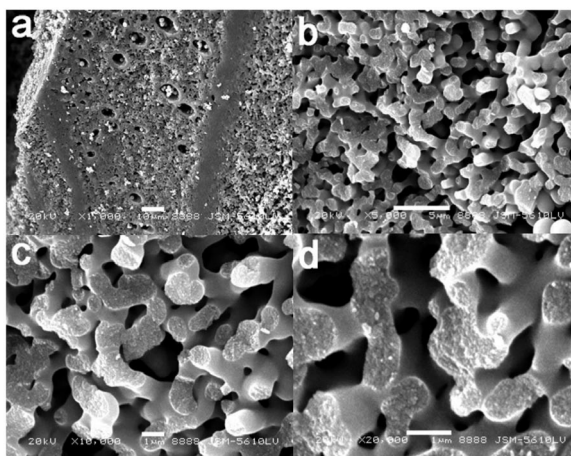


Fig. 23 SEM images of hierarchically sponge-like macro-/mesoporous titania prepared at 180 °C for 24 h [207].

Self-formation phenomenon of porous hierarchy and the progen concept

To study the formation mechanism, a new preparation pathway was carried out by the authors [196,197,199]. A controlled polymerization of zirconium tetrapropoxide was performed by adding this chemical dropwise onto a 2-ml aqueous film in order to follow the macrostructure formation “in situ” by optical microscopy (OM). Figure 24 depicts OM images (1–7) showing the different steps of the process leading to hierarchically meso-/macroporous zirconia and one SEM picture (8) of the final product obtained by this experiment. Polymerization was rapid, yielding a gelatinous and translucent shell on the external surface of the droplet as soon as the zirconium alkoxide came into contact with water (1). Only a very short moment after, the particle began to spin itself spontaneously and very rapidly, generating a strong agitation in the medium (2–6). It was clearly observed that the liquid inside of the droplet with a translucent and gelatinous shell was moving with some force. The core of the particle then swelled progressively leading to a specific “sombbrero”-like morphology. The stirring continued and some parts of the smooth envelope broke away from the particle (8). The macroporosity was then observable below this smooth surface. These observations clearly suggest a mechanism based on the synergy between the polymerization kinetics of the inorganic precursors and the hydrodynamic flow of the solvent.

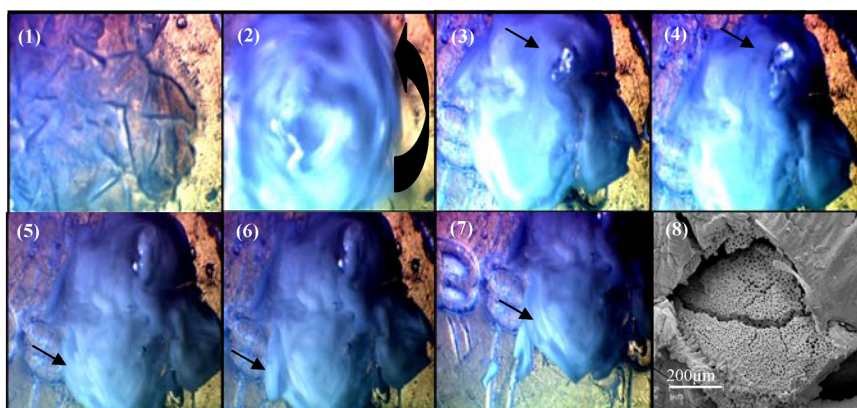


Fig. 24 OM (1–7) and SEM (8) images of the controlled polymerization of a $Zr(OC_3H_7)_4$ drop [197].

At the end of the reaction and after drying, “sombbrero”-shaped particles were obtained (Fig. 25A). A close glance at the broken part of the particle clearly showed the homogeneously distributed uniform macro openings of 0.5–2 μm (Figs. 25B, C, and D). The picture with higher magnification illustrated that the walls around the macro-openings were formed by the uniform-sized particles of 100–500 nm (secondary particles) which were themselves composed of even smaller particles of around 20 nm (primary particles). The aggregation of these small particles should certainly generate mesoporosity [196,197,199].

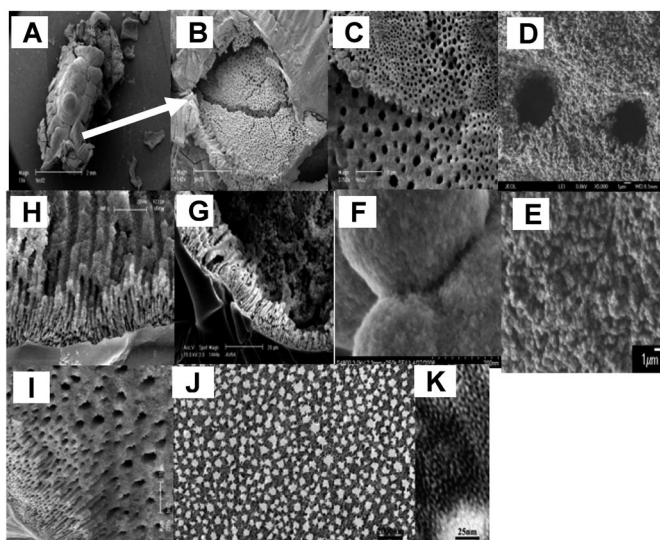


Fig. 25 SEM and TEM images of the controlled polymerization of a $\text{Zr}(\text{OC}_3\text{H}_7)_4$ drop [199].

The formation of these new hierarchical meso-/macroporous ZrO_2 structures can be explained as follows: The zirconium propoxide drop added into the aqueous medium polymerizes very quickly, leading to a smooth ZrO_2 shell which acts as a semipermeable membrane. The alcohol and water molecules released suddenly from the structure by spontaneous polymerization can only be expelled inward toward the center of the droplet due to the formation of this dense translucent gelatinous and semipermeable shell. All these alcohol and water molecules gather together leading to the formation of larger water/ethanol macrochannels inside the structure. Meanwhile, polymerization generates large amounts of ZrO_2 nanoparticles, giving the interparticular mesoporosity. Inside these nanoparticles, another micro- or mesoporosity is formed. The amount of water/ethanol trapped inside the particle creates high pressures, which in turn cause the splitting of the particle, resulting in hierarchical meso-(micro-)/macroporous ZrO_2 particles with funnel-like shaped macropores oriented perpendicularly to the smooth particle surface as observed by SEM. The mechanism is illustrated in Fig. 26.

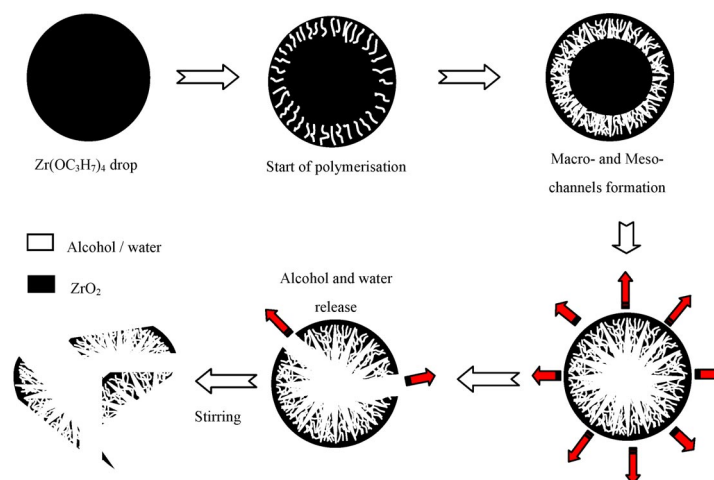


Fig. 26 Schematic representation for the formation of meso-(micro-)/macroporous zirconia [197].

The key point of this novel synthesis process is the very high rate at which the hydrolyzed metal alkoxides undergo condensation reactions in aqueous solution. Alcohol molecules can be generated suddenly as soon as the metal alkoxide precursor is in contact with the water molecules. The molecules of alcohol will increase in quantity as the reaction progresses because one metal alkoxide molecule can produce at least two more alcohol molecules. These alcohol molecules can be considered as the “porogen” in the generation of the funnel-like macrochannels with hierarchically mesostructured porous walls. This new process could be of great interest and is a significant advance toward the understanding of the formation mechanism of these hierarchically structured porous materials. This process could be adopted for the large-scale preparation of mesoporous membranes with well-oriented, funnel-like, straight macrochannels which interconnect with the mesoporous shell and pores walls. The process could be used to target new functional materials with very sophisticated architectures. Instead of alcohol molecules as the self-generated “porogen”, it is possible to imagine other precursors which can generate and release “porogen molecules” in liquid and even in gas form. The formation mechanism of these meso-/macroporous structures has been discussed in depth in recent papers [196,197,199]. These metal oxides with a hierarchical meso-/macroporous network have additional benefits as a result of the enhanced access to the mesopores by the regular macrochannel array. Porous aluminosilicate materials have been widely used as acid catalysts and supports [208]. The introduction of a hierarchical architecture in porous materials will enhance their performance further. By using alkoxides of silicon and aluminum in a controlled aqueous solution, without surfactant, the spontaneous formation of aluminosilicate macrochannels with tunable mesoporous walls occurred [195]. A comprehensive description on the formation mechanism and porogen concept was given in refs. [196,197,199]. Combined with template replication methods, hierarchically structured multimodal meso-/macroporous carbon materials have been prepared by carefully adjusting the amount of the carbon precursor. This new kind of mesoporous carbon with funnel-shaped macrochannels possesses aligned and uniformly sized macrochannels with interconnected, well-organized, wormhole-like hierarchically porous walls with unique mesoporosities centered at 3, 10–17, and 25–50 nm [196,197,199] (Fig. 27).

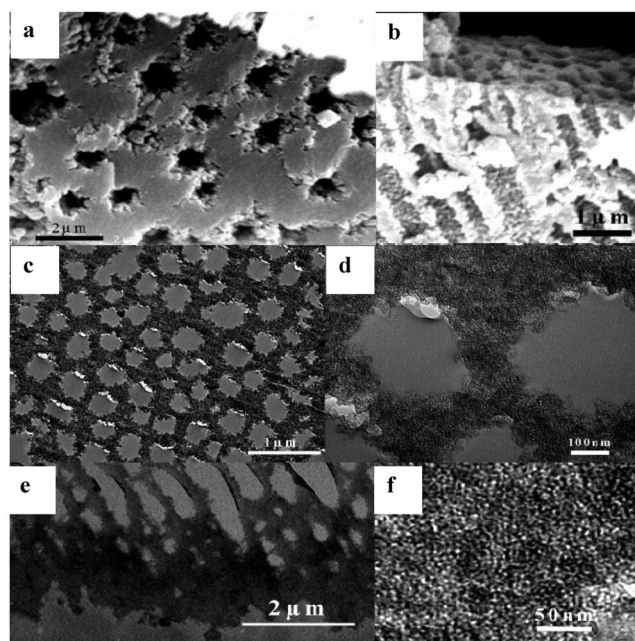


Fig. 27 (a, b) SEM images and (c–f) cross-sectional TEM images of hierarchically macroporous carbon replica [198].

Thus, the macrochannels are generated by a sudden release of alcohol molecules, and the mesoporosity is due to the assembly of ZrO_2 nanoparticles which quickly form. A third porosity can be found inside these nanoparticles. New experiments were carried out with several alkoxides [$\text{Ti}(\text{OR})_4$, $\text{Al}(\text{OR})_3$, $\text{Y}(\text{OR})_3$, $\text{Nb}(\text{OR})_5$, $\text{Ta}(\text{OR})_5$, $\text{Si}(\text{OR})_4$]. Similar to the polymerization of $\text{Zr}(\text{OC}_3\text{H}_7)_4$, hierarchically bimodal even trimodal porous structures were obtained for most of the above-mentioned alkoxides, but the macropore diameters, meso- and micropore sizes, surface areas, and porous volumes were influenced by the type of inorganic precursor. Moreover, it is important to notice that no macropores were obtained when the electronegativity of the metal was higher than 1.8 [e.g., $\text{Si}(\text{OR})_4$] whatever the corresponding alkoxide. This means that the spontaneous formation of macrochannels depends on the kinetics of the nucleophilic attack of water molecules on the partial positively charged metal.

Prolongation of self-formation procedure

Micro-/macroporous Ti oxides

Titanium oxides are interesting compositions because of their applications in photocatalysis and as catalyst supports. Mesoporous Ti oxides have been prepared by several surfactant-assisted pathways, with control of channel structure, texture and morphology. The synthesis of high surface area hierarchical micro-/macroporous titanium oxide materials was carried out by a controlled polymerization of titanium alkoxide inorganic sources [$\text{Ti}(\text{OC}_2\text{H}_5)_4$, $\text{Ti}(\text{OC}_3\text{H}_7)_4$, $\text{Ti}(\text{OC}_4\text{H}_9)_4$]. The synthesized particles are around 1 mm in size and exhibit a regular array of funnel-like sinusoidal macrochannels (Fig. 28a). The macropore sizes range from 0.3 to 1.5 μm , and their walls are formed by an agglomeration of microporous TiO_2 nanoparticles. This microporosity is confirmed by type I N_2 adsorption-desorption isotherms (Fig. 28b). Very high surface areas (400–470 m^2/g) are obtained for each titanium alkoxide precursor, and the pore size distribution is always centered in the microporous range [185].

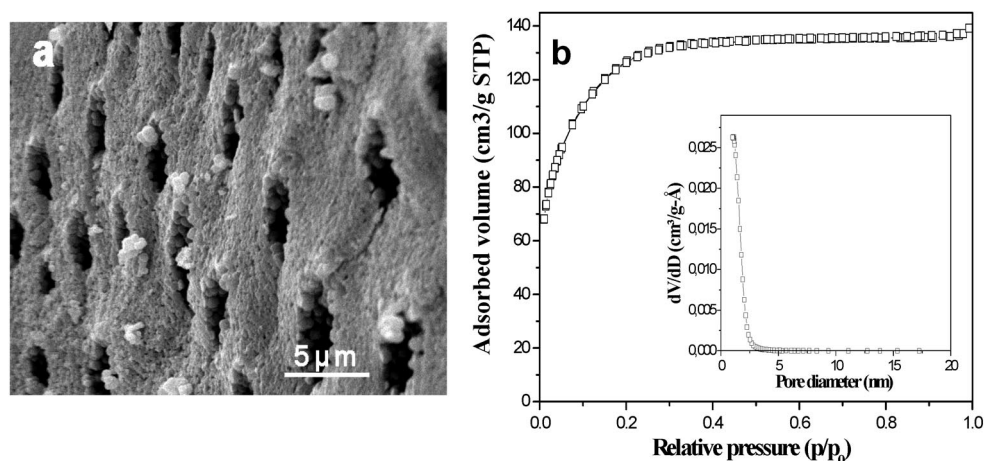


Fig. 28 SEM micrography (a), adsorption-desorption isotherm and pore size distribution (b) of a micro-/macroporous TiO_2 synthesized via $\text{Ti}(\text{OEt})_4$ [185].

Ethylene photodegradation was employed as a probe reaction to evaluate the photocatalytic activity of these new meso-/macroporous TiO_2 structures. The results reveal a photocatalytic activity of 60 %, much higher than that of commercial P25 Titania powders. It is evident that these new TiO_2 bimodal meso-/macroporous structures hold promise as catalysts and catalyst supports.

Micro-/macroporous niobium oxides

A few years ago, Antonelli reported the synthesis of meso-/macroporous niobium oxides by a NaCl-promoted vesicle templating method using a niobium ethoxide/amine gel. These materials have macropore sizes in the 200–300 nm range and mesopores of around 2 nm. The formation mechanism was discussed above. Despite their interesting structural and textural properties, these structures can only be prepared by a fairly complex synthesis route. The self-formation pathway used for zirconia and titania was applied in the design of hierarchical micro-/macroporous niobium oxides. The preparations were carried out at different starting pH values (2, 7, and 12). In each case, the synthesized Nb₂O₅ particles were mainly 100 μm in size with a regular array of parallel macropores (Fig. 29a). The macropores extended throughout almost the entire particle, and their diameter ranged from 0.3 to 10 μm. Moreover, high-magnification TEM images reveal accessible micropores in the macropore walls. XRD patterns show broad features in the 2θ range of 20–40° and 40–60°, indicating the global amorphous nature of the niobium oxide frameworks. Type II isotherms, typical of macroporous structures, are observed, and the BET surface areas are 144, 127, and 73 m² g for the syntheses carried out in acidic, neutral, and basic media, respectively. Finally, thermogravimetry/differential thermal analysis (TG/DTA) demonstrates the strong acidic properties of the hydrated hierarchical micro-/macroporous niobium oxide. In the future, these new solid catalysts will be tested in low-temperature catalytic reactions.

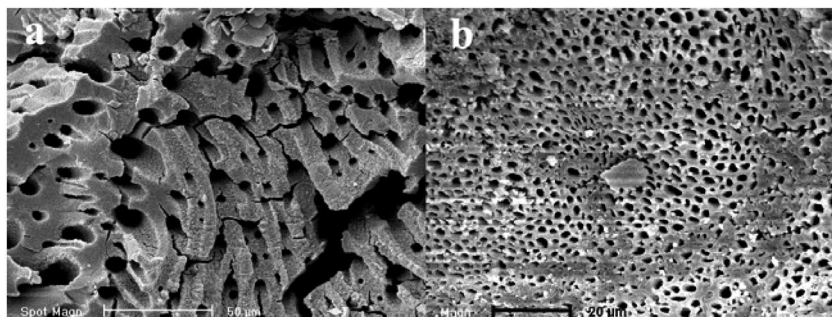


Fig. 29 SEM pictures of the micro-/macroporous niobia (a) and meso-/macroporous yttria (b) [185].

Meso-/macroporous yttrium oxides

Yttrium oxides possess unique properties, the main ones being a higher melting temperature than many other well-known oxides, a wide energy bandgap, high values of electrical resistivity, and electric strength. The self-formation strategy was also applied to the preparation of hierarchically porous Y₂O₃ by a controlled polymerization of yttrium butoxide in aqueous media. For each pH value tested, the synthesized Y₂O₃ particles are 0.5–2 μm in size and are covered by a smooth surface, cracked in some places. Higher-resolution SEM observations of the fissured particles reveal a macrostructure below the smooth surface (Fig. 29b). It is worth mentioning that synthesis yields as well as the amount of macropores per particle continuously decrease with increasing initial synthesis pH values. The macropores are funnel-like shaped and parallel to each other, as observed for the previous zirconia and their diameters range from 1–5, 2–8, and 5–10 μm, respectively, for syntheses carried out in acidic, neutral, and basic media. In each case, the macropore walls are formed by aggregation of mesostructured nanoparticles, giving a supplementary interparticular porosity centered at 30 nm. As for all the previously described compositions, the meso-/macroporous yttria structures are amorphous at the atomic scale. BET surface areas of 85, 74, and 94 m² g are obtained for samples prepared in acidic, neutral, and basic media, respectively, and the BJH pore size distributions are quite broad and centered in the mesopore range, 3–7 nm for syntheses carried out in acidic and neutral media and 5–15 nm in an alkaline medium. These

new macro-/mesoporous yttrium oxide structures will be tested as catalysts or supports in a wide range of chemical reactions.

Combination of self-formation and templated synthesis

Interestingly, the bimodal nanoporous aluminosilicates with a hierarchically macroporous core inside an ordered mesoporous shell were successfully synthesized via a one-pot reaction. This was achieved through a combination of surfactant templating and the self-formation phenomenon of porous hierarchy [209]. In this case, the aluminosilicate ester $[(\text{Bu}^t\text{O})_2\text{Al}-\text{O}-\text{Si}-(\text{OEt})_3]$ can be used for the synthesis of bimodal nanoporous aluminosilicates with hierarchically macroporous core/mesoporous shell. The use of this aluminosilicate ester, containing various hydrolysis rates, renders the precise control of this novel structure possible [209]. In fact, the hydrolysis of the $\text{Al}-(\text{Bu}^t\text{O})_2$ side is very rapid and the interior macroporous structure is easily self-formed, even under template-free conditions [210]. Conversely, the hydrolysis of the $\text{Si}-(\text{OEt})_3$ side is slow and can assemble together with TMOS (tetramethyl orthosilicate), a supplementary silica source, around surfactant micelles (CTMAB) to form an ordered mesoporous structure at the surface of the cores. Therefore, the novel nanosized spheres with a foam-like macroporous core (self-formation) and an ordered mesoporous shell (templated synthesis) can be obtained (Figs. 30a–d). This study illustrates that the self-formation procedure is quite versatile and can

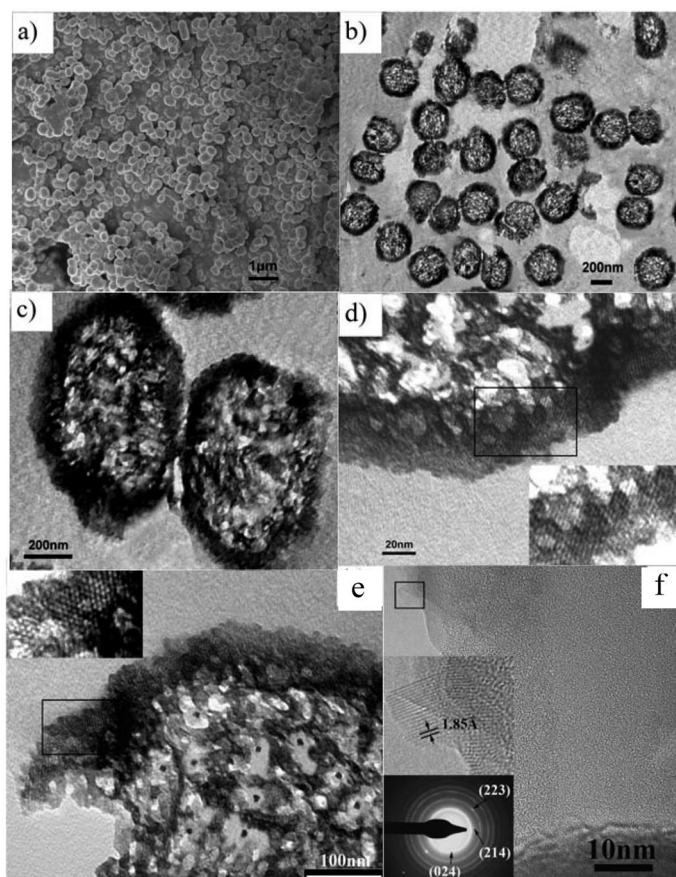


Fig. 30 SEM, TEM, and HRTEM images of calcined novel nanosized spheres (a–d) with foam-like macroporous core (self-formation) and ordered mesoporous shell (templated synthesis) and the nanoreactor (e, f) encapsulated Fe_2O_3 with this novel core-shell structure. The inserts in the HRTEM images are the corresponding SAED patterns taken from lots of particles [209].

be combined with any other synthesis to achieve the synthesis of more sophisticated hierarchically porous materials. Additionally, the synthetic method that produces core-shell structures was applied in the design of a nanoreactor by the encapsulation and crystallization of metal oxide nanoparticles inside a core-shell structure (Figs. 30e,f). The ultimate advantage of this new core-shell structure is that the mesoporous shell allows the diffusion of chemical reagents toward the inside of the structure and prevents leaching of the active metal oxide nanocrystals, formed in the macroporous core.

CONCLUSIONS AND OUTLOOK

Recent progress made in the template synthesis of hierarchically porous materials was reviewed. By using appropriate synthetic procedures, porous materials with hierarchical pore dimensions and pore structures were synthesized. These templated synthesis methods involve the use of a dual supermolecular assembly of amphiphilic polymers, surfactants employed with the macrotemplates such as solid particles, liquid drops, and air bubbles, surfactants employed with additional chemical and physical methods, controlled phase-separation, template replication, and innovative self-formation processes. In most synthesis methods, multiporosity involving micro-, meso-, and macroporosity can be easily and independently adjusted. For example, micro- and mesostructures are generally decided by small organic molecular and amphiphile supermolecules and inorganic precursors, while the macroporous structures are controlled by the nature of the selected macrotemplates. Furthermore, the macroscopic morphology can also be designed to be of monoliths, thin films, membranes, or spheres, depending on the demands of various practical applications. The hierarchical materials synthesized with interconnected hierarchically porous structures and defined morphologies can be expected to combine reduced resistance to diffusion and high surface areas for adsorption and reaction, particularly for large molecular guest species (e.g., biomolecules). However, the design of such multiscaled porous materials with controllable ordered pore structures and crystalline framework still remains a challenge. The structural stability and framework crystallinity may also be important issues for these hierarchical materials, regarding their practical applications.

The self-formation mechanism of the spontaneous assembly of hierarchically porous metal oxides is still not totally clear to date, although more progress has been made in the design and synthesis of hierarchically porous materials employing a porogene concept and other templated synthesis strategies. The development of new and versatile synthesis methods is still interesting and necessary. Moreover, utilizing these hierarchically porous oxide materials as templates to make replicas of hierarchical carbon or other composites is attracting much attention and would be a new and interesting research direction.

Nature yields many examples of self-formation hierarchy and is therefore the source of inspiration for the development of several new strategies [211,212]. The combination of multiscaled porosity, integrated into one moldable body, holds promise for improving overall reactions as well as adsorption/separation, and/or structural properties. Some practical applications of these attractive meso-/macroporous materials have recently been emerging, including separation, catalysis, fuel cell electrode materials, biomaterial engineering, controlled drug delivery devices, and membrane reactors. The enhanced performances in catalysis, adsorption, and separation have been achieved in these hierarchical porous materials, and can be attributed to the minimization of intradiffusion resistance and a high surface area for active site dispersion. Moreover, their intriguing properties can grant the extension of applications to gas sensing [213], since the multiscale porous architecture promotes gas diffusion and increases the active surface area [214]. The utilization of hierarchically meso-/macroporous materials as catalyst supports has shown its superiority in different oxidation and water gas shift reactions [215–222]. It is reasonable to expect that further modification of the individual porosities and intricate morphologies, as well as surface functionalization of the hierarchically porous materials, may open new perspectives for applications when considering the combined properties.

ACKNOWLEDGMENTS

This work was realized in the frame of the Belgian Federal Government (Belspo PAI-IAP project, INANOMAT, P6/17 and Belgium-Viet Nam bilateral cooperation project, BL/13/V11). The work was also supported by the National Natural Science Foundation of China (Grant Nos. 50625208, 20773097, and 20877061), and also financially supported by the National Basic Research Program of China (Grant Nos. 2007CB613302 and 2009CB939704). X. Y. Yang thanks the University of Namur for a doctoral fellowship and FNRS (Fonds National de la Recherche Scientifique in Belgium) for a “Chargé de recherche” position. B.-L. Su thanks the Chinese central government for an “Expert of the state” position in the frame of the program of “Thousands Talents” and the Ministry of Education of China for the “Changjiang scholar” position at Wuhan University of Technology.

REFERENCES

1. A. Stein. *Adv. Mater.* **15**, 763 (2003).
2. M. Davis. *Nature* **417**, 813 (2002).
3. G. Soler-Illia, C. Sanchez, B. Lebeau, J. Patarin. *Chem. Rev.* **102**, 4093 (2002).
4. C. Kresge, M. Leonowicz, W. Roth, J. Vartuli, J. Beck. *Nature* **359**, 710 (1992).
5. J. Beck, J. Vartuli, W. Roth, M. Leonowicz, C. Kresge, K. Schmitt, C. Chu, D. Olsen, E. Sheppard, S. McCullen, J. Higgins, J. Schlenker. *J. Am. Chem. Soc.* **114**, 10834 (1992).
6. D. Zhao, J. Feng, Q. Huo, N. Melosh, G. Fredrickson, B. Chmelka, G. Stucky. *Science* **279**, 548 (1998).
7. D. Zhao, Q. Huo, J. Feng, B. Chmelka, G. Stucky. *J. Am. Chem. Soc.* **120**, 6024 (1998).
8. B. Holland, C. Blanford, A. Stein. *Science* **281**, 538 (1998).
9. C. Blanford, H. Yan, R. Schroden, M. Al-Daous, A. Stein. *Adv. Mater.* **13**, 401 (2001).
10. H. Yan, C. Blanford, B. Holland, W. Smyrl, A. Stein. *Chem. Mater.* **12**, 1134 (2000).
11. J. Fan, C. Yu, J. Lei, Q. Zhang, T. Li, B. Tu, W. Zhou, D. Zhao. *J. Am. Chem. Soc.* **127**, 10794 (2005).
12. J. Yu, J. Yu, M. Leung, W. Ho, B. Cheng, X. Zhao, J. Zhao. *J. Catal.* **217**, 69 (2003).
13. N. Tsubaki, Y. Zhang, S. Sun, H. Mori, Y. Yoneyama, X. Li, K. Fujimoto. *Catal. Commun.* **2**, 311 (2001).
14. Z. Y. Yuan, J. L. Blin, B. L. Su. *Chem. Commun.* 504 (2002).
15. S. Bagshaw. *Chem. Commun.* 1785 (1999).
16. X. Wang, T. Dou, Y. Xiao. *Chem. Commun.* 1035 (1998).
17. J. Sun, Z. Shan, T. Maschmeyer, J. Moulijn, M. Coppens. *Chem. Commun.* 2670 (2001).
18. J. El Haskouri, D. De Zárte, C. Guillem, J. Latorre, M. Caldés, A. Beltrán, D. Beltrán, A. Descalzo, G. Rodríguez-López, R. Martínez-Mañez, M. Marcos, P. Amoros. *Chem. Commun.* 330 (2002).
19. J. Sun, Z. Shan, T. Maschmeyer, M. Coppens. *Langmuir* **19**, 8395 (2003).
20. M. Antonietti, B. Berton, C. Goltner, H. Hentze. *Adv. Mater.* **10**, 154 (1998).
21. M. Groenewolt, M. Antonietti, S. Polarz. *Langmuir* **20**, 7811 (2004).
22. R. Weberskirch, O. Nuyken. *J. Macromol. Sci., Pure Appl. Chem.* **A36**, 843 (1999).
23. K. Stahler, J. Selb, F. Candau. *Langmuir* **15**, 7565 (1999).
24. P. Barthelemy, V. Tomao, J. Selb, Y. Chaudier, B. Pucci. *Langmuir* **18**, 2557 (2002).
25. S. Avera, C. Boissiere, D. Grosso, T. Asakawa, C. Sanchez, M. Linden. *Chem. Commun.* 1630 (2004).
26. X. Yang, S. Zhang, Z. Qiu, G. Tian, Y. Feng, F. Xiao. *J. Phys. Chem. B* **108**, 4696 (2004).
27. Y. Zhou, M. Antonietti. *Adv. Mater.* **15**, 1452 (2003).
28. T. Brezesinski, C. Erpen, K. Iimura, B. Smarsly. *Chem. Mater.* **17**, 1683 (2005).
29. Y. Zhou, J. Schattka, M. Antonietti. *Nano Lett.* **4**, 477 (2004).

30. B. Trewyn, C. Whitman, V. Lin. *Nano Lett.* **4**, 2139 (2004).
31. Y. Zhou, M. Antonietti. *Chem. Commun.* 2564 (2003).
32. D. Kuang, T. Brezesinski, B. Smarsly. *J. Am. Chem. Soc.* **126**, 10534 (2004).
33. O. Sel, D. Kuang, M. Thommes, B. Smarsly. *Langmuir* **22**, 2311 (2006).
34. P. Yang, T. Deng, D. Zhao, P. Feng, D. Pine, B. Chmelka, G. Whitesides, G. Stucky. *Science* **282**, 2244 (1998).
35. B. Holland, L. Abrams, A. Stein. *J. Am. Chem. Soc.* **121**, 4308 (1999).
36. B. Lebeau, C. Fowler, S. Mann, C. Farcet, B. Charleux, C. Sanchez. *J. Mater. Chem.* **10**, 2105 (2000).
37. Q. Luo, L. Li, B. Yang, D. Zhao. *Chem. Lett.* **378**, 24 (2000).
38. Z. Yang, K. Qi, J. Rong, L. Wang, Z. Liu, Y. Yang. *Chin. Sci. Bull.* **46**, 1785 (2001).
39. G. Gundiah. *Bull. Mater. Sci.* **24**, 211 (2001).
40. S. Vaudreuil, M. Bousmina, S. Kaliaguine, L. Bonneviot. *Adv. Mater.* **13**, 1310 (2001).
41. C. Danumah, S. Vaudreuil, L. Bonneviot, M. Bousmina, S. Giasson, S. Kaliaguine. *Micropor. Mesopor. Mater.* **44–45**, 241 (2001).
42. C. Oh, Y. Baek, S. Ihm. *Adv. Mater.* **17**, 270 (2005).
43. R. Schroden, C. Blanford, B. Melde, B. Johnson, A. Stein. *Chem. Mater.* **13**, 1074 (2001).
44. T. Sen, G. Tiddy, J. Casci, M. Anderson. *Angew. Chem., Int. Ed.* **42**, 4649 (2003).
45. T. Sen, G. Tiddy, J. Casci, M. Anderson. *Chem. Mater.* **16**, 2044 (2004).
46. F. Li, Z. Wang, N. Ergang, C. Fyfe, A. Stein. *Langmuir* **23**, 3996 (2007).
47. D. Zhao, P. Yang, B. Chmelka, G. Stucky. *Chem. Mater.* **11**, 1174 (1999).
48. H. Nishihara, S. Mukai, D. Yamashita, H. Tamon. *Chem. Mater.* **17**, 683 (2005).
49. R. Caruso, J. Schattka. *Adv. Mater.* **12**, 1921 (2000).
50. R. Caruso, M. Antonietti. *Adv. Funct. Mater.* **12**, 307 (2002).
51. P. Giunta, R. Washington, T. Campbell, O. Steinbock, A. Stiegman. *Angew. Chem., Int. Ed.* **43**, 1505 (2004).
52. S. Davis, S. Burkett, N. Mendelson, S. Mann. *Nature* **385**, 420 (1997).
53. F. Meldrum, R. Seshadri. *Chem. Commun.* 29 (2000).
54. D. Yang, L. Qi, J. Ma. *Adv. Mater.* **14**, 1543 (2002).
55. G. Cook, P. Timms, C. Goeltner-Spickermann. *Angew. Chem., Int. Ed.* **42**, 557 (2003).
56. S. Hall, H. Bolger, S. Mann. *Chem. Commun.* 2784 (2003).
57. V. Valtchev, M. Smiaili, A. Faust, L. Vidal. *Angew. Chem., Int. Ed.* **42**, 2782 (2003).
58. V. Valtchev, M. Smiaili, A. Faust, L. Vidal. *Chem. Mater.* **16**, 1350 (2003).
59. Y. Shin, L. Wang, J. Chang, W. Samuels, G. Exarhos. *Stud. Surf. Sci. Catal.* **146**, 447 (2003).
60. L. Wang, Y. Shin, W. Samuels, G. Exarhos, I. Moudrakovski, V. Terskikh, J. Ripmeester. *J. Phys. Chem. B* **107**, 13793 (2003).
61. X. Yang, Z. Li, B. Liu, A. Klein-Hofmann, G. Tian, Y. Feng, Y. Ding, D. Su, F. Xiao. *Adv. Mater.* **18**, 410 (2006).
62. L. Huang, H. Wang, C. Hayashi, B. Tian, D. Zhao, Y. Yan. *J. Mater. Chem.* **13**, 666 (2003).
63. Y. Shin, C. Wang, G. Exarhos. *Adv. Mater.* **17**, 73 (2005).
64. W. Ogasawara, W. Shenton, S. Davis, S. Mann. *Chem. Mater.* **12**, 2835 (2000).
65. V. Pedroni, P. Schulz, M. de Ferreira, M. Morini. *Colloid Polym. Sci.* **278**, 964 (2000).
66. M. Iwasaki, S. Davis, S. Mann. *J. Sol-Gel Sci. Technol.* **32**, 99 (2004).
67. D. Walsh, L. Arcelli, T. Ikoma, J. Tanaka, S. Mann. *Nat. Mater.* **2**, 386 (2003).
68. A. Imhof, D. Pine. *Nature* **389**, 948 (1997).
69. A. Imhof, D. Pine. *Adv. Mater.* **10**, 697 (1998).
70. S. Schacht, Q. Huo, I. Voigt-Martin, G. Stucky, F. Schuth. *Science* **273**, 768 (1996).
71. T. Sen, G. Tiddy, J. Casci, M. Anderson. *Micropor. Mesopor. Mater.* **78**, 255 (2005).
72. T. Sen, G. Tiddy, J. Casci, M. Anderson. *Chem. Commun.* 2182 (2003).
73. H. Zhang, G. Hardy, M. Rosseinsky, A. Cooper. *Adv. Mater.* **15**, 78 (2003).

74. F. Carn, A. Colin, M. Achard, H. Deleuze, E. Sellier, M. Birot, R. Backov. *J. Mater. Chem.* **14**, 1370 (2004).
75. Z. Y. Yuan, T. Z. Ren, B. L. Su. *Adv. Mater.* **15**, 1462 (2003).
76. H. Yang, H. Zeng. *Angew. Chem., Int. Ed.* **43**, 5206 (2004).
77. D. Antonelli. *Micropor. Mesopor. Mater.* **33**, 209 (1999).
78. S. Bagshaw. *Chem. Commun.* 767 (1999).
79. F. Carn, A. Colin, M. Achard, H. Deleuze, Z. Saadi, R. Backov. *Adv. Mater.* **16**, 140 (2004).
80. F. Carn, A. Colin, M. Achard, H. Deleuze, C. Sanchez, R. Backov. *Adv. Mater.* **17**, 62 (2005).
81. K. Suzuki, K. Ikari, H. Imai, *J. Mater. Chem.* **13**, 1812 (2003).
82. H. Maekawa, J. Esquena, S. Bishop, C. Solans, B. Chmelka. *Adv. Mater.* **15**, 591 (2003).
83. L. Huerta, C. Guillern, J. Latorre, A. Beltrán, D. Beltrán, P. Amoros. *Chem. Commun.* 1448 (2003).
84. L. Huerta, C. Guillern, J. Latorre, A. Beltrán, D. Beltrán, P. Amoros. *Solid State Sci.* **7**, 405 (2005).
85. A. Ryoo, C. Ko, M. Kruk, V. Antochshuk, M. Jaroniec. *J. Phys. Chem. B* **104**, 11465 (2000).
86. M. Impéror-Clerc, P. Davidson, A. Davidson. *J. Am. Chem. Soc.* **122**, 11925 (2000).
87. P. Ravikovitch, A. Neimark. *J. Phys. Chem. B* **105**, 6817 (2001).
88. A. Galarneau, H. Cambon, F. Di Renzo, R. Ryoo, M. Choi, F. Fajula. *New J. Chem.* **27**, 73 (2003).
89. Y. Goto, S. Inagaki. *Chem. Commun.* 2121 (2000).
90. P. Van Der Voort, P. Ravikovitch, K. De Jong, A. Neimark, A. Janssen, M. Benjelloun, E. Van Bavel, P. Cool, B. Weckhuysen, E. Vansant. *Chem. Commun.* 1010 (2002).
91. Y. Hsu, Y. Hsu, H. Hsu, C. Yang. *Chem. Mater.* **19**, 1120 (2007).
92. K. Nakanishi. *J. Porous Mater.* **4**, 67 (1997).
93. Y. Sato, K. Nakanishi, K. Hirao, H. Jinnai, M. Shibayama, Y. Melnichenko, G. Wignall. *Colloids Surf., A* **187–188**, 117 (2001).
94. K. Nakanishi, Y. Sato, Y. Ruyat, K. Hirao. *J. Sol-Gel Sci. Technol.* **26**, 567 (2003).
95. J. Smått, S. Schunk, M. Linden. *Chem. Mater.* **15**, 2354 (2003).
96. S. Murai, K. Fujita, K. Nakanishi, K. Hirao. *J. Phys. Chem. B* **108**, 16670 (2004).
97. R. Takahashi, S. Sato, T. Sodesawa, K. Suzuki, M. Tafu, K. Nakanishi, N. Soga. *J. Am. Ceram. Soc.* **84**, 1968 (2001).
98. J. Konishi, K. Fujita, K. Nakanishi, K. Hirao. *Mater. Res. Soc. Symp. Proc.* **788**, L8.14.1 (2004).
99. K. Nakanishi, Y. Kobayashi, T. Amatani, K. Hirao, T. Kodaira. *Chem. Mater.* **16**, 3652 (2004).
100. T. Amatani, K. Nakanishi, K. Hirao, T. Kodaira. *Chem. Mater.* **17**, 2114 (2005).
101. Z. Shi, Y. Feng, L. Xu, S. Da, Y. Ren. *Micropor. Mesopor. Mater.* **68**, 55 (2004).
102. N. Huesing, C. Raab, V. Torma, A. Roig, H. Peterlik. *Chem. Mater.* **15**, 2690 (2003).
103. N. Huesing, C. Raab, V. Torma. *Mater. Res. Soc. Symp. Proc.* **775**, 9 (2003).
104. D. Brandhuber, V. Torma, C. Raab, H. Peterlik, A. Kulak, N. Huesing. *Chem. Mater.* **17**, 4262 (2005).
105. H. Lin, Y. Cheng, C. Mou. *Chem. Mater.* **10**, 3772 (1998).
106. H. Lin, C. Mou. *Acc. Chem. Res.* **35**, 927 (2002).
107. H. Lin, C. Mou, S. Liu, C. Tang. *Chem. Commun.* 1970 (2001).
108. Y. Li, J. Shi, Z. Hua, H. Chen, M. Ruan, D. Yan. *Nano Lett.* **3**, 609 (2003).
109. Y. Zhu, J. Shi, W. Shen, X. Dong, J. Feng, M. Ruan, Y. Li. *Angew. Chem., Int. Ed.* **44**, 5083 (2005).
110. G. Buchel, K. Unger, K. Matsumoto, K. Tsutsumi. *Adv. Mater.* **10**, 1036 (1998).
111. C. Graf, D. Vossen, A. Imhof, A. van Blaaderen. *Langmuir* **19**, 6693 (2003).
112. V. Valtchev. *Chem. Mater.* **14**, 956 (2002).
113. G. Zhu, S. Qiu, O. Terasaki, Y. Wei. *J. Am. Chem. Soc.* **123**, 7723 (2001).
114. A. Dong, Y. Wang, Y. Tang, N. Ren, Y. Zhang, Z. Gao. *Chem. Mater.* **14**, 3217 (2002).
115. M. Ohmori, E. Matijevic. *J. Colloid Interface Sci.* **160**, 288 (1993).

116. S. Marinakos, J. Novak, L. Brousseau, A. House, E. Edeki, J. Feldhaus, D. Feldheim. *J. Am. Chem. Soc.* **121**, 8518 (1999).
117. J. Yu, J. Kim, S. Lee, J. Mbindyo, B. Martin, T. Mallouk. *Chem. Commun.* 2445 (2000).
118. L. Dahne, S. Leporatti, E. Donath, H. Mohwald. *J. Am. Chem. Soc.* **123**, 5431 (2001).
119. F. Caruso, M. Spasova, A. Susha, M. Giersig, R. Caruso. *Chem. Mater.* **13**, 109 (2001).
120. K. Kamata, Y. Lu, Y. Xia. *J. Am. Chem. Soc.* **125**, 2384 (2003).
121. F. Caruso. *Chem.—Eur. J.* **6**, 413 (2000).
122. M. Kim, S. Yoon, B. K. Sohn, J. Kim, C. Shin, T. Hyeon, J. Yu. *Micropor. Mesopor. Mater.* **63**, 1 (2003).
123. F. Caruso. *Adv. Mater.* **13**, 11 (2001).
124. Z. Dai, L. Dahne, H. Mohwald, B. Tiersch. *Angew. Chem., Int. Ed.* **41**, 4019 (2002).
125. J. Yu, S. Yoon, Y. Lee, K. Yoon. *J. Phys. Chem. B* **109**, 7040 (2005).
126. Y. Wang, F. Caruso. *Chem. Commun.* 1528 (2004).
127. H. Chen, J. Gao, M. Ruan, J. Shi, D. Yan. *Micropor. Mesopor. Mater.* **76**, 209 (2004).
128. K. Lin, L. Chen, M. Prasad, C. Cheng. *Adv. Mater.* **16**, 1845 (2004).
129. Y. Liu, W. Zhang, T. Pinnavaia. *J. Am. Chem. Soc.* **122**, 8791 (2000).
130. Y. Liu, W. Zhang, T. Pinnavaia. *Angew. Chem., Int. Ed.* **40**, 1255 (2001).
131. Y. Liu, T. Pinnavaia. *Chem. Mater.* **14**, 3 (2002).
132. Z. Zhang, Y. Han, L. Zhu, R. Wang, Y. Yu, S. Qiu, D. Zhao, F. Xiao. *Angew. Chem., Int. Ed.* **40**, 1258 (2001).
133. F. Xiao, Y. Han, Y. Yu, X. Meng, M. Yang, S. Wu. *J. Am. Chem. Soc.* **124**, 888 (2002).
134. Y. Han, S. Wu, Y. Sun, D. Li, F. Xiao. *Chem. Mater.* **14**, 1144 (2002).
135. D. Trong On, S. Kaliaguine. *Angew. Chem., Int. Ed.* **40**, 3248 (2001).
136. D. Trong On, D. Lutic, S. Kaliaguine. *Micropor. Mesopor. Mater.* **44–45**, 435 (2001).
137. D. Trong On, S. Kaliaguine. *Angew. Chem., Int. Ed.* **41**, 1036 (2002).
138. D. Trong On, S. Kaliaguine. *J. Am. Chem. Soc.* **125**, 618 (2003).
139. Y. Xia, R. Mokaya. *J. Mater. Chem.* **14**, 3427 (2004).
140. J. Yu, W. Liu, H. Yu. *Cryst. Growth Des.* **8**, 930 (2008).
141. J. Yu, X. Yu. *Environ. Sci. Technol.* **42**, 4902 (2008).
142. J. Yu, H. Guo, S. Davis, S. Mann. *Adv. Funct. Mater.* **16**, 2035 (2006).
143. J. Yu, H. Yu, H. Guo, M. Li, S. Mann. *Small* **4**, 87 (2008).
144. H. Yu, J. Yu, S. Liu, S. Mann. *Chem. Mater.* **19**, 4327 (2007).
145. J. Yu, S. Liu, M. Zhou. *J. Phys. Chem. C* **112**, 2050 (2008).
146. J. Yu, S. Liu, H. Yu. *J. Catal.* **249**, 59 (2007).
147. J. Beck, J. Vartuli, G. Kennedy, C. Kresge, W. Roth, S. Schramm. *Chem. Mater.* **6**, 1816 (1994).
148. A. Karlsson, M. Stocker, R. Schmidt. *Micropor. Mesopor. Mater.* **27**, 181 (1999).
149. N. Petkov, M. Holzl, T. Metzger, S. Mintova, T. Bein. *J. Phys. Chem. B* **109**, 4485 (2005).
150. S. van Donk, A. Janssen, J. Bitter, K. de Jong. *Catal. Rev.* **45**, 297 (2003).
151. C. Jacobsen, C. Madsen, J. Houzvicka, I. Schmidt, A. Carlsson. *J. Am. Chem. Soc.* **122**, 7116 (2000).
152. Y. Tao, H. Kanoh, K. Kaneko. *J. Am. Chem. Soc.* **125**, 6044 (2003).
153. S. Kim, H. Shah, T. Pinnavaia. *Chem. Mater.* **15**, 1664 (2003).
154. I. Schmidt, A. Boisen, E. Gustavsson, K. Stahl, S. Pehrson, S. Dahl, A. Carlsson, C. Jacobsen. *Chem. Mater.* **13**, 4416 (2001).
155. A. Sakthivel, A. Huang, W. Chen, Z. Lan, K. Chen, T. Kim, R. Ryoo, A. Chiang, S. Liu. *Chem. Mater.* **16**, 3168 (2004).
156. A. Dong, Y. Wang, Y. Tang, Y. Zhang, N. Ren, Z. Gao. *Adv. Mater.* **14**, 1506 (2002).
157. F. Xiao, L. Wang, C. Yin, K. Lin, Y. Di, J. Li, R. Xu, D. Su, R. Schlogl, T. Yokoi, T. Tatsumi. *Angew. Chem., Int. Ed.* **45**, 3090 (2006).
158. M. Choi, H. Cho, R. Srivastava, C. Venkatesan, D. Choi, R. Ryoo. *Nat. Mater.* **5**, 718 (2006).

159. F. Rodriguez-Reinoso. In *Introduction in Carbon Technology*, H. Marsh, E. A. Heintz, F. Rodriguez-Reinoso (Eds.), p. 35, Universidad de Alicante, Secretariado de publicaciones, Alicante, Spain (1997).
160. S. Subramoney. *Adv. Mater.* **10**, 1157 (1998).
161. J. Knox, B. Kaur, G. Millward. *J. Chromatogr.* **352**, 3 (1986).
162. J. Lee, J. Kim, T. Hyeon. *Chem. Commun.* 1138 (2003).
163. K. Gierszal, M. Jaroniec. *Chem. Commun.* 2576 (2004).
164. J. Lee, J. Kim, J. Kim, H. Jia, M. Kim, J. Kwak, S. Jin, A. Dohnalkova, H. Park, H. Chang, P. Wang, J. Grate, T. Hyeon. *Small* **1**, 744 (2005).
165. A. Taguchi, J. Smätt, M. Linden. *Adv. Mater.* **15**, 1209 (2003).
166. S. Yoon, K. Sohn, J. Kim, C. Shin, J. Yu, T. Hyeon. *Adv. Mater.* **14**, 19 (2002).
167. M. Kim, K. Sohn, H. Na, T. Hyeon. *Nano Lett.* **2**, 1383 (2002).
168. C. Yu, J. Fan, B. Tian, D. Zhao, G. Stucky. *Adv. Mater.* **14**, 1742 (2002).
169. A. Fuertes. *J. Mater. Chem.* **13**, 3085 (2003).
170. A. Zakhidov, R. Baughman, Z. Iqbal, C. Cui, I. Khayrullin, S. Dantas, J. Marti, V. Ralchenko. *Science* **282**, 897 (1998).
171. J. Yu, S. Yoon, G. Chai. *Carbon* **39**, 1422 (2001).
172. Z. Lei, Y. Zhang, H. Wang, Y. Ke, J. Li, F. Li, J. Xing. *J. Mater. Chem.* **11**, 1975 (2001).
173. S. Kang, J. Yu, M. Kruk, M. Jaroniec. *Chem. Commun.* 1670 (2002).
174. J. Yu, S. Kang, S. Yoon, G. Chai. *J. Am. Chem. Soc.* **124**, 9382 (2002).
175. S. Yoon, G. Chai, S. Kang, J. Yu, K. Gierszal, M. Jaroniec. *J. Am. Chem. Soc.* **127**, 4188 (2005).
176. A. Lu, J. Smatt, S. Backlund, M. Linden. *Micropor. Mesopor. Mater.* **72**, 59 (2004).
177. Z. Shi, Y. Feng, L. Xu, S. Da, M. Zhang. *Carbon* **41**, 2677 (2003).
178. G. Chai, I. Shin, J. Yu. *Adv. Mater.* **16**, 2057 (2004).
179. A. Lu, W. Schmidt, A. Taguchi, B. Spliethoff, B. Tesche, F. Schuth. *Angew. Chem., Int. Ed.* **41**, 3489 (2002).
180. M. Kang, S. Yi, H. Lee, J. Yi, J. Kim. *Chem. Commun.* 1944 (2002).
181. J. Roggenbuck, M. Tiemann. *J. Am. Chem. Soc.* **127**, 1096 (2005).
182. X. Zhang, K. Tu, Y. Xie, C. Tung, S. Xu. *Adv. Mater.* **18**, 1905 (2006).
183. G. Che, B. Lakshmi, E. Fisher, C. Martin. *Nature* 393 (1998).
184. X. Chen, M. Steinhart, C. Hess, U. Gosele. *Adv. Mater.* **18**, 2153 (2006).
185. B. L. Su, A. Leonard, Z. Y. Yuan. *C. R. Chim.* **8**, 713 (2005).
186. J. L. Blin, A. Leonard, Z. Yuan, L. Gigot, A. Vantomme, A. Cheetham, B. L. Su. *Angew. Chem., Int. Ed.* **42**, 2872 (2003).
187. Z. Y. Yuan, A. Vantomme, A. Leonard, B. L. Su. *Chem. Commun.* 1558 (2003).
188. T. Z. Ren, Z. Y. Yuan, B. L. Su. *Langmuir* **20**, 1531 (2004).
189. A. Leonard, J. L. Blin, B. L. Su. *Chem. Commun.* 2568 (2003).
190. Z. Y. Yuan, T. Z. Ren, A. Vantomme, B. L. Su. *Chem. Mater.* **16**, 5096 (2004).
191. Z. Y. Yuan, T. Z. Ren, A. Azoune, J. Pireaux, B. L. Su. *Chem. Mater.* **18**, 1753 (2006).
192. T. Z. Ren, Z. Y. Yuan, A. Azoune, B. L. Su. *Langmuir* **22**, 3886 (2006).
193. T. Z. Ren, Z. Y. Yuan, B. L. Su. *Chem. Commun.* 2730 (2004).
194. T. Z. Ren, Z. Y. Yuan, B. L. Su. *Chem. Phys. Lett.* **388**, 46 (2004).
195. A. Leonard, B. L. Su. *Chem. Commun.* 1674 (2004).
196. A. Leonard, B. L. Su. *Colloids Surf., A* **300**, 129 (2007).
197. A. Vantomme, A. Leonard, Z. Y. Yuan, B. L. Su. *Colloids Surf., A* **300**, 70 (2007).
198. A. Vantomme, A. Leonard, Z. Y. Yuan, B. L. Su. *Key Eng. Mater.* **336–338**, 1933 (2007).
199. B. L. Su, A. Vantomme, L. Surahy, R. Pirard, J. Pirard. *Chem. Mater.* **19**, 3325 (2007).
200. A. Vantomme, Z. Y. Yuan, B. L. Su. *New J. Chem.* **28**, 1083 (2004).
201. Z. Y. Yuan, B. L. Su. *J. Mater. Chem.* **16**, 663 (2006).
202. W. Deng, M. Toepke, B. Shanks. *Adv. Funct. Mater.* **13**, 61 (2003).

203. H. Chen, J. Gu, J. Shi, Z. Liu, J. Gao, M. Ruan, D. Yan. *Adv. Mater.* **17**, 2010 (2005).
204. A. Collins, D. Carriazo, S. Davis, S. Mann. *Chem. Commun.* 568 (2004).
205. W. Deng, B. Shanks. *Chem. Mater.* **17**, 3092 (2005).
206. J. Yu, Y. Su, B. Cheng. *Adv. Funct. Mater.* **17**, 1984 (2007).
207. J. Yu, L. Zhang, B. Cheng, Y. Su. *J. Phys. Chem. C* **111**, 10582 (2007).
208. A. Corma. *Chem. Rev.* **97**, 2373 (1997).
209. X. Y. Yang, Y. Li, G. Van Tendeloo, F. Xiao, B. L. Su. *Adv. Mater.* **21**, 1368 (2009).
210. X. Y. Yang, A. Vantomme, A. Lemaire, F. Xiao, B. L. Su. *Adv. Mater.* **18**, 2117 (2006).
211. S. Mann. *Chem. Commun.* 1 (2004).
212. J. Aizenberg, J. Weaver, M. Thanawala, V. Sunder, D. Morse, P. Fratzl. *Science* **309**, 275 (2005).
213. Y. Shimizu, T. Hyodo, M. Egashira. *Catal. Surv. Asia* **8**, 127 (2004).
214. C. Martinez, B. Hockey, C. Montgomery, S. Semancik. *Langmuir* **21**, 7937 (2005).
215. Z. Y. Yuan, V. Idakiev, A. Vantomme, T. Tabakova, T. Z. Ren, B. L. Su. *Catal. Today* **131**, 203 (2008).
216. V. Idakiev, T. Tabakova, A. Naydenov, Z. Y. Yuan, B. L. Su. *Appl. Catal., B* **63**, 178 (2006).
217. V. Idakiev, T. Tabakova, Z. Y. Yuan, B. L. Su. *Appl. Catal., A* **270**, 135 (2004).
218. V. Idakiev, L. Ilieva, D. Andreeva, J. Blin, L. Gigot, B. L. Su. *Appl. Catal., A* **243**, 25 (2003).
219. H. Tidahy, M. Hosseini, S. Siffert, R. Cousin, J. Lamonier, A. Aboukais, B. L. Su, J. Giraudon, G. Leclercq. *Catal. Today* **137**, 335 (2008).
220. J. Giraudon, M. T. Nguyen, B. G. Leclercq, S. Siffert, J. Lamonier, F. A. Aboukais, A. Vantomme, B. L. Su. *Catal. Today* **137**, 379 (2008).
221. M. Hosseini, S. Siffert, H. L. Tidahy, R. Cousin, J. Lamonier, A. Aboukais, A. Vantomme, M. Roussel, B. L. Su. *Catal. Today* **122**, 391 (2007).
222. H. Tidahy, S. Siffert, J. Lamonier, E. Zhilinskaya, A. Aboukais, Z. Y. Yuan, A. Vantomme, B. L. Su, X. Canet, G. De Weireld, M. Frere, T. N'Guyen, J. Giraudon, G. Leclercq. *Appl. Catal., A* **310**, 61 (2006).